The Lateglacial to Early Holocene tephrochronological record from Esmeer, Drenthe, the Netherlands

Universiteit Utrecht

Marjolein Saskia Veneman

Master thesis *Earth Structure & Dynamics*

Date: 31 July 2019

Student number: 3514633

First supervisor: Dr. W.Z. Hoek

Second supervisor: Prof. dr. M.R. Drury

Content

Abstract

Tephrochronology is a powerful tool in geomorphological and climatological research, since volcanic deposits can function as time-parallel markers over large areas. This thesis presents the search for tephra layers in a Lateglacial – Early Holocene sediment sequence from lake Esmeer, the Netherlands. A targeted search is made for the 12.5 ka Laacher See Tephra, originating from the German Laacher See volcano, and the 12.1 ka Vedde Ash, originating from the Icelandic Katla volcano. Although some glass-like shards were observed at the target depths for Laacher See Tephra, no evidence is found for a positive correlation. At target Vedde Ash depths, a cryptotephra is found. Its major, minor, and trace element concentrations are established by the use of WDS-EPMA and LA-ICP-MS and resemble the well-established rhyolitic component of Vedde Ash. A pollen and LOI diagram of the sediment sequence of lake Esmeer provided an estimated deposition age in the mid Younger Dryas, allowing a correlation to Vedde Ash. The pollen diagram also allows a reconstruction of the paleoenvironment at the time of Vedde Ash deposits in the area around lake Esmeer.

Preface and acknowledgements

This research is part of my master programme Earth Structure & Dynamics at Utrecht University, in which I specialised in geochemistry. My fascination for volcanism led to a research topic comprising tephra deposits, which introduced me into the world of physical geography as well. This research allowed me to dive into this topic, while still making use of my previous specialisation geochemistry. This report will therefore be a combination of both geochemistry as well as physical geography.

I am grateful to the many people who supported me during my research. This research would not have succeeded without their help, interest and enthusiasm. First and foremost, I would like to thank my supervisor Wim Hoek, whose support, friendliness and interest for this research has been of great value. His enthusiasm for researching geomorphological topics has been both supportive and invigorating to me. I also would like to thank my second supervisor Martyn Drury, who took the time to advise me about the geochemical chapters of this research. Also many thanks to Paul Mason, Tilly Bouten and Helen de Waard, whose expertise was highly appreciated during my geochemical analyses and data processing. Thanks to Maaike Zwier, who researched the Esmeer core as well, for accompanying me both to the NAC 2018 and during the many hours of counting tephra shards. Thanks to Arjen van Silfhout, who spent his precious time on improving the English language of this report. Finally, thanks to all of the students who accompanied me to the library while I was writing this report. I owe you lots of coffee.

1. Introduction

Volcanos act as large vents on the Earth's surface where molten rock, gasses and debris are emitted from the planet's interior. One of the materials produced during volcanic eruptions is tephra, fragmental volcanic material regardless of composition or size. Such material gets injected into the air during eruptions and prevailing wind can carry small sized tephra over far distances. Precipitation and gravitational fallout causes deposition of airborne tephra. The further away from the source volcano, the fewer and smaller the tephra deposits will be.

If tephra deposits are stored and well preserved in stratigraphical records, they can form time parallel markers across the area reached by the tephra fallout (neglecting any minor time differences in fallout time for different regions). Such time parallel markers are powerful tools in geomorphological research and climate reconstructions. To be able to synchronize sequences from different locations based on a tephra deposit, this tephra must be identified as originating from the same volcanic eruption. Volcanic eruptions often have unique geochemical fingerprints, meaning its produced material is chemically distinct. By establishing the geochemical composition and comparing this to other geochemical data, a correlation to a particular volcanic system can be made. In case geochemical compositions of different tephra horizons are similar, additional information like deposition age is helpful in establishing the correct source volcanic eruption, and a tephrochronological record can be established (e.g. Lane et al., 2012a; Lane et al., 2012b).

The potential of tephrochronology has led to many tephra related studies and the establishment of a tephro-stratigraphical framework. To fully use the power of tephrochronology, tephra data concerning geochemical concentrations and deposit locations must be easily accessible, which is one of the benefits of a tephro-stratigraphical framework (Turney et al., 2004).

Currently, only limited research is conducted to tephra deposits in the Netherlands. The first and only tephra related research for the Lateglacial in the Netherlands is performed by Davies et al. (2005) who found Vedde Ash and possibly Laacher See Tephra in a sediment sequence spanning the Lateglacial – Interglacial transition, cored from Kostverloren Veen in Drenthe. To help improve the tephrostratigraphical framework, this research aims to establish the presence of tephra layers in a Lateglacial – Early Holocene sediment record from Esmeer, Drenthe, the Netherlands. The research question is: Which tephra layers can be traced and identified in the Lateglacial – Early Holocene record of the Esmeer (Drenthe)? The scope of this research, searching and identifying tephra layers in the Lateglacial – Early Holocene record of Esmeer, is confined to finding two tephra horizons: Vedde Ash and Laacher See Tephra.

2. Tephrochronology

Tephrochronology is a geochronological technique using layers of tephra from a known and dated single volcanic eruption as a means to link sites together at fixed points in time (neglecting any variance in tephra fallout time). Most useful for tephrochronology is tephra that (a) is chemically distinct, so it can be recognised by its geochemical composition, and (b) was able to spread over a large distance, so that a significant area is affected by its depositions.

Multiple distinct tephra depositions in the Late Termination have been recognized and used for tephrochronology during the last decades. In the north-western parts of Europe, Icelandic volcanic systems like Hekla and Katla produce the majority of useful tephra deposits, including the well-known Vedde Ash (Mangerud et al., 1984) and Saksunarvatn tephra (Waagstein & Jóhansen, 1968; Mangerud et al., 1986). The Eifel region in Germany also produced a distinct and wide spread ash layer, named Laacher See Tephra (Bogaard & Schmincke, 1986) as a result of the eruption of the Laacher See volcano. In the previous century, the majority of tephra horizons encountered in European sites were found as visible layers in sediment records, due to large sized shards and a high tephra shard concentration. Since tephra fallout is the highest close to its source volcano, such visible encounters of tephra were often limited to a confined area close to a volcano. This also limited the potential of tephrochronology. The rise of new separation techniques in the late 1990s changed this position and allows establishing the presence of tephra layers that are smaller in shard size and lower in tephra shard concentration. Such tephra deposits invisible to the naked eye are called cryptotephra (derived from the Greek word *kryptein,* meaning *to hide*) as recommended by Lowe and Hunt (2001). This development has led to the discovery of new tephra layers, like the Borrobol tephra (Turney et al., 1997) which is currently only encountered as cryptotephra. It has also led to an extension of the distribution area of already known tephra layers, by finding far-travelled cryptotephra deposits related to tephra previously encountered as visible layers.

Finding (crypto)tephra horizons can strengthen climate reconstruction research by providing time parallel markers, for example in pollen diagrams. Fluctuations in paleoenvironments can be studied on a detailed scale if multiple identified tephra horizons and therefore time markers are available. Comparisons between different research sites can be made as well if similar tephra horizons are found across a larger area.

This chapter describes the creation and development of a tephrochronological framework. It furthermore provides detailed information regarding the two tephra layers to which this research is confined: the Laacher See Tephra and Vedde Ash, as based on earlier tephra related research in the Netherlands by Davies et al., 2005.

2.1 Tephrochronological framework

Tephrochronology as a new means of establishing precise ages arose due to two major forces (Turney et al., 2004). The first one was the publication of ice-core records, showing that the Last Termination (18,000 – 9000 ^{14}C yr BP) suffered from environmental changes more complex and sudden than previously thought. Alley et al. (1993) describe the results from the Greenland ice core GISP2, that show the Younger Dryas ended abruptly with a short timescale of possibly less than 20 years. If such short timescales are involved, a precise method is required to reconstruct a sequence of events during the Last Termination, preferably to a decadal time-scale. Few geological dating techniques can unravel past environmental events at this high level of precision, therefore a new method was desirable. The second major force leading to the rise of tephrochronology was the growing realisation of the difficulties that surround radiocarbon dating, the method most frequently used to date Last Termination events. Such difficulties include contamination and stratigraphical disturbance of sedimentary layers, and the lack of a strong ^{14}C calibration model (Lowe & Walker, 2000).

The aforementioned reasons led to the consideration of tephrochronology as a tool to improve Last Termination models. To fully use the potential of tephrochronology, it is essential that tephra data is collected in a proper way and that results of tephra related research is easily accessible. This is one of the benefits of what is started as the INTIMATE project (INTegration of Ice-core-MArine and TErrestrial records). This project was designed to further develop the collaboration between the ice-core, marine and terrestrial communities, aiming to integrate proxy climate records for the Last Termination from around the North Atlantic realm. (Turney et al., 2004; Walker, 2016). Since its foundation, the INTIMATE programme has expanded geographically and now includes the entire Atlantic basin, Australia and New Zealand. The temporal framework is also extended and now covers the early Holocene and the Last Glacial cycle as well (Lowe et al., 2008; Walker, 2016). An example of a centralized tephra database as recommended by Turney et al. (2004) and others, is Tephrabase, launched on the internet in 1995. This website functions as a centralized platform to facilitate the identification, correlation, and dating of tephra deposits (Newton, 1996; Newton et al., 2007).

A draft protocol for synchronizing tephrochronological research was suggested by Turney et al. (2004). For inclusion in a centralised tephra database, tephra research should include detailed information concerning site location, stratigraphical context, tephra characteristics (*inter alia* shard morphology and colour), geochemical data, and tephra age. Several procedures for tephra dating and geochemical analysis are suggested as well. Besides the methods used during the geochemical analysis, the extraction method to isolate tephra shards from sediment records should be appropriate and synchronized. Therefore, a laboratory protocol was suggested by Blockley et al. (2005), who introduced a step-by-step guideline to isolate tephra shards including

floating separation techniques. Both the recommended protocol of Turney et al. (2004) and the laboratory guideline of Blockley et al. (2005) will be used as framework for this research.

2.2 Laacher See Tephra

Laacher See Tephra (LST) originates from a phaeton-Plinian eruption of the Laacher See volcano in the eastern Eifel volcanic field (Germany). Its first and only eruption has been dated at 12,880 ± 40 varve years BP in Lake Meerfelder Maar (Brauer et al., 1999) or 12,937 ± 23 cal. a BP, based on a multi-site radiocarbon age model (Ramsey et al., 2015). During its explosive eruption circa 6.3 km^3 magma, equivalent to 20 km^3 of tephra (Harms and Schmincke, 2000) was produced and the eruption column is estimated to have reached a height of circa 22-40 km in the Plinian phases (Schmincke et al., 1999). Three main dispersal plumes of phonolitic to mafic phonolitic ash were sent in multiple directions, predominantly to the north-east, south-west and south. This broad distribution is one of the reasons why LST is such a crucial marker in Lateglacial deposits in Central Europe.

The produced tephra is subdivided into three categories, (1) the Lower (LLST), (2) Middle (MLST) and (3) Upper (ULST) Laacher See Tephra, mainly as a result of a strongly zoned magma chamber. The MLST is further categorized into subcategories A, B and C. The categories differ in chemical composition, lithology, eruptive mechanisms, and areal extent (Bogaard and Schmincke, 1984). Deposited tephra varies from highly evolved phenocryst-poor, phonolitic white pumice in LLST (inferred top of the magma chamber) to more crystal-rich, mafic, gray pumice in MLST and ULST (inferred lower parts of the magma chamber) (Schmincke et al., 1999). The geochemical composition of LST is well determined and slightly varies per category. SiO_2 is the largest component of LST and varies between 56 to 61 wt%, other major elements are Al_2O_3 (20-23 wt%), Na_2O (7-12 wt%), K_2O (5-8 wt%), FeO (1-3 wt%), CaO (0.3-2 wt%), and MnO (0.1-0.5 wt%) (Bogaard and Schminke, 1984). The average SiO_2 content of LST increases systematically from basal LLST toward MLST C and varies unsystematically in MLST C to ULST. Elements that increase in average content as well from LLST to ULST are FeO, K_2O and CaO. Elements that decrease in average content from LLST to ULST are Al_2O_3 and Na_2O and MnO.

The distribution of LST fans over Europe is visible in figure 1. Map *a* shows the main tephra lobes in correlation to their chemical composition. Map *b* shows an isopach map of the main tephra lobes in correlation to the amount of distributed material. As can be seen in both maps, LST is found over large parts of Europe. The tephra seems to be divided into three main lobes with a characteristic mixture of chemical compositions. The first lobe is spread to a North-East direction, containing several large fans of MLST. A second large lobe is spread to the South, containing fans of both MLST and ULST. A minor fan is seen in a South-West direction, also containing MLST.

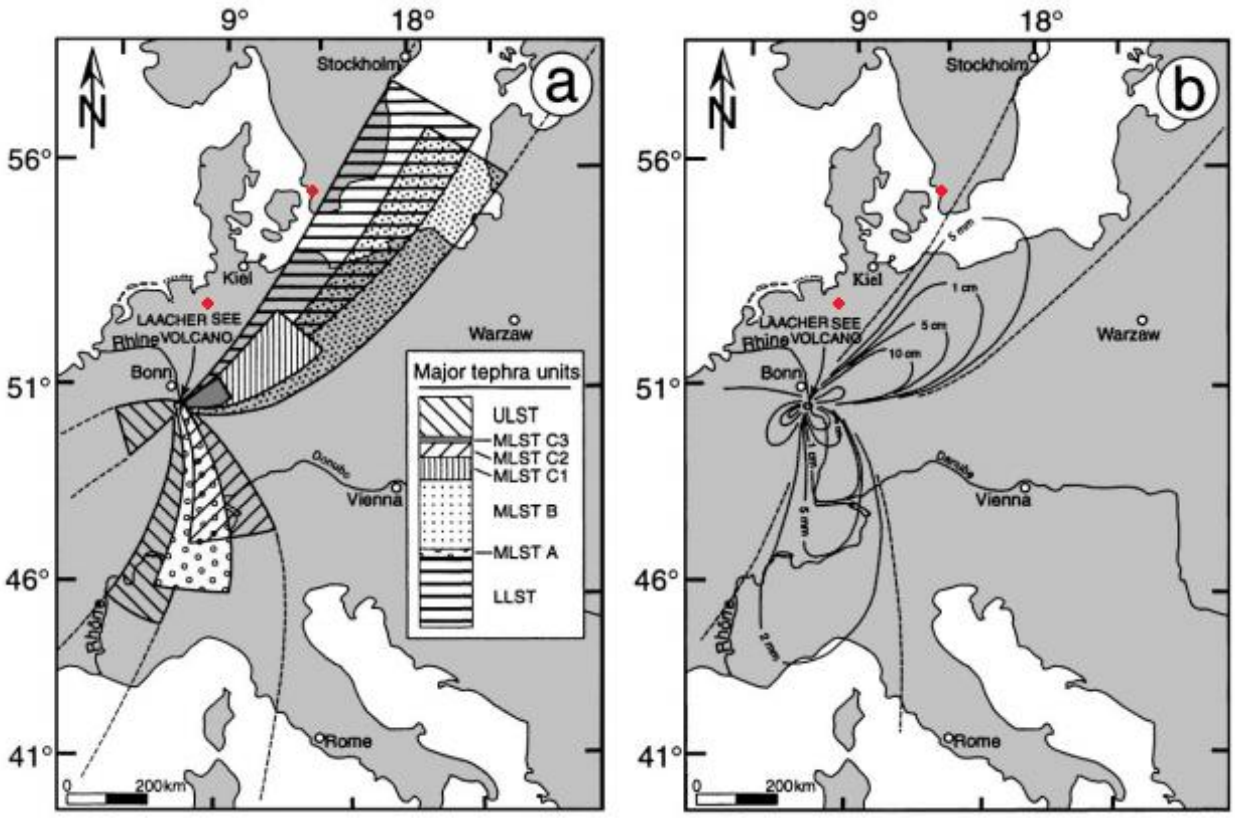

Fig. 1: *Maps showing distribution area of Laacher See Tephra. Map A shows the distribution of the major tephra units ULST, MLST and LLST in three major lobes. The isochron map B shows how much tephra material is distributed per major lobe. Red dots indicate more recent LST discoveries that fall out of the major lobes. Slightly modified after Schminke et al., 1999.*

Since the creation of these maps, several other locations containing LST are discovered that slightly fall out of the distribution range in figure 1. Examples are lake Hämelsee (Jones et al., 2018) in northern Germany and Körslättamorssen in southernmost Sweden (Larsson and Wastegård, 2018). Both locations are (slightly) more westward than the large lobe in northern direction, indicated by the red dots in figure 1. The LST deposit in the lake Hämelsee succession occurred as a visible, circa 500 µm-thick and light grey layer, whereas the deposit in Körslättamorssen was a high concentration cryptotephra (ca. 65 500 shards cm^{-3}). The LST found in lake Hämelsee shows a correlation to the upper phase of LST, which was previously assumed to only have spread in a southward direction. So not only did LST spread more westward than previously thought, the types of LST present in this lobe are more diverse as well.

Fig. 2: *Map showing the LST distribution as known by Tephrabase. All red marks indicate a single research site at which LST is encountered. Not all encountered LST shards are geochemically analysed. Retrieved on 30 July 2019 from www.tephrabase.org.*

To show the current state of known LST occurrences, a map has been downloaded from Tephrabase.org. This map (downloaded on the 30th of July 2019) is visible in figure 2 and indicates all locations containing LST as currently known by Tephrabase. Only a limited number (16) of these LST occurrences have been geochemically analysed as well. The single red marker in the Netherlands indicates the location of Davies et al. (2005) who speculated about the presence of LST in Kostverloren Veen. The amount of encountered tephra was too little to be geochemically analysed, therefore it could not be confirmed with absolute certainty whether the observed shards were truly LST shards. Nonetheless, this occurrence of tephra has been included in the Tephrabrase data records.

Because of the possibility of a more widespread distribution of LST and the potential presence of LST in the Netherlands, it is interesting to look for far-travelled LST in an extended area, including the Netherlands. Finding LST in Esmeer (the Netherlands) and establishing its geochemical composition would expand the currently known distribution area.

2.3 Vedde Ash

Besides the Laacher See Tephra, another type of volcanic tephra is frequently researched and encountered in the tephra record of the Lateglacial – Early Holocene period. This tephra is called Vedde Ash and originates from the Icelandic Katla system. The first mentioning of Vedde Ash in scientific literature is by Mangerud et al. (1984) who describes a visible grey-coloured bed of glass shards preserved in multiple sediment records near Ålesund, western Norway. Because of the large quantity of glass shards it was believed to be the result of a large and explosive volcanic eruption, making it a useful tephra layer for tephrochronology. Recent research has dated the eruption responsible for the spreading of Vedde Ash to 12,023 ± 43 cal. a BP using radio carbon dating (Bronk Ramsey et al., 2015), and at 12 140 ± 43 varve years BP (Lane et al., 2015).

Whereas Vedde Ash was first mainly discovered as visible beds in sediment records, the development of analytical and separation techniques significantly changed this. Due to density separation techniques, cryptotephra can be extracted out of sediments. Therefore, far-travelled Vedde Ash located beyond the limits of visible records can now be detected as well (Turney et al., 1997). Vedde Ash has reached a considerably large area, stretching from north-west Russia (Wastegård et al., 2000) towards Greenland (Mortensen et al., 2005) in an east-west direction, and from northern Norway (Vorren et al., 2009) to Italy (Lane et al., 2012a) in a north-south direction.

The correlation of most occurrences of Vedde Ash has been based upon the geochemical composition of the encountered glass shards. The major and minor element concentration of Vedde Ash is well defined and led to a distinction between a rhyolitic and basaltic end member. The rhyolitic end member is the most common one and has been encountered all over the distribution area of Vedde Ash. Its chemical composition is quite consistent with circa 68-72 wt% SiO_2, 12.5-13.7 wt% Al_2O_3, 4.0-5.0 wt% Na_2O, 3.0-3.5 wt% Ka_2O, 1.0-1.5 wt% CaO, and some other minor elements of generally <1 wt% (e.g. Mangerud et al., 1984; Blockley et al., 2007; Lane et al., 2012b). In contrary to the major and minor element concentration, he trace element concentration of Vedde Ash is less well researched, but is currently characterized by 73-89 ppm Rb, 750-940 ppm Zr, and 110-130 ppm Nb (Lane et al., 2012b).

The basaltic end member is restricted to the northern part of the distribution area and is found in e.g. Greenland (Mortensen et al., 2005), Norway (Mangerud et al., 1984) and in Scotland (Davies et al., 2001). The basaltic Vedde Ash is a Fe-Ti transitional alkali basalt, characterised by an anhydrous glass composition of circa 47 wt% SiO_2, 14 wt% FeO, 13 wt% Al_2O_3, 10 wt% CaO, 3 wt% Na_2O and 0.7 wt% K_2O (e.g. Mangerud et al., 1984; Lane et al., 2012b). The trace element concentration is characterized by 14-17 ppm Rb, 210-250 ppm Zr and 32-36 ppm Nb (Lane et al., 2012b). Intermediate forms of Vedde Ash are found on some locations, including Kråkenes (Lane et al., 2012b) and Ålesund (Mangerud et al., 1984) in Norway.

However, as Lane et al. (2012b) shows, the major and minor element composition of glass shards alone might not be sufficient for a positive correlation to Vedde Ash. The Icelandic Katla volcanic system has erupted multiple times and produced tephra that is very similar in major and minor element composition. Lately, three other far-travelled tephra layers have been discovered that originate from the Katla volcano and have a similar major and minor element composition as the rhyolitic end member of Vedde Ash. These include the Suðuroy tephra dated at circa 8 ka BP (Wastegård, 2002), the AF 555 tephra dated at 11.2-11.8 ka BP (Matthews et al., 2011), and the Dimna Ash dated at > 15 ka BP (Koren et al., 2008). Also the trace element concentration of Dimna Ash is very similar to the rhyolitic Vedde Ash (Lane et al, 2012b). The most convenient method to distinguish these compositional similar tephra's is by their deposit age.

To give an impression of the current state of Vedde Ash findings, figure 3 shows a map marking all locations where Vedde Ash (both rhyolitic and basaltic) has been encountered until 2012. The

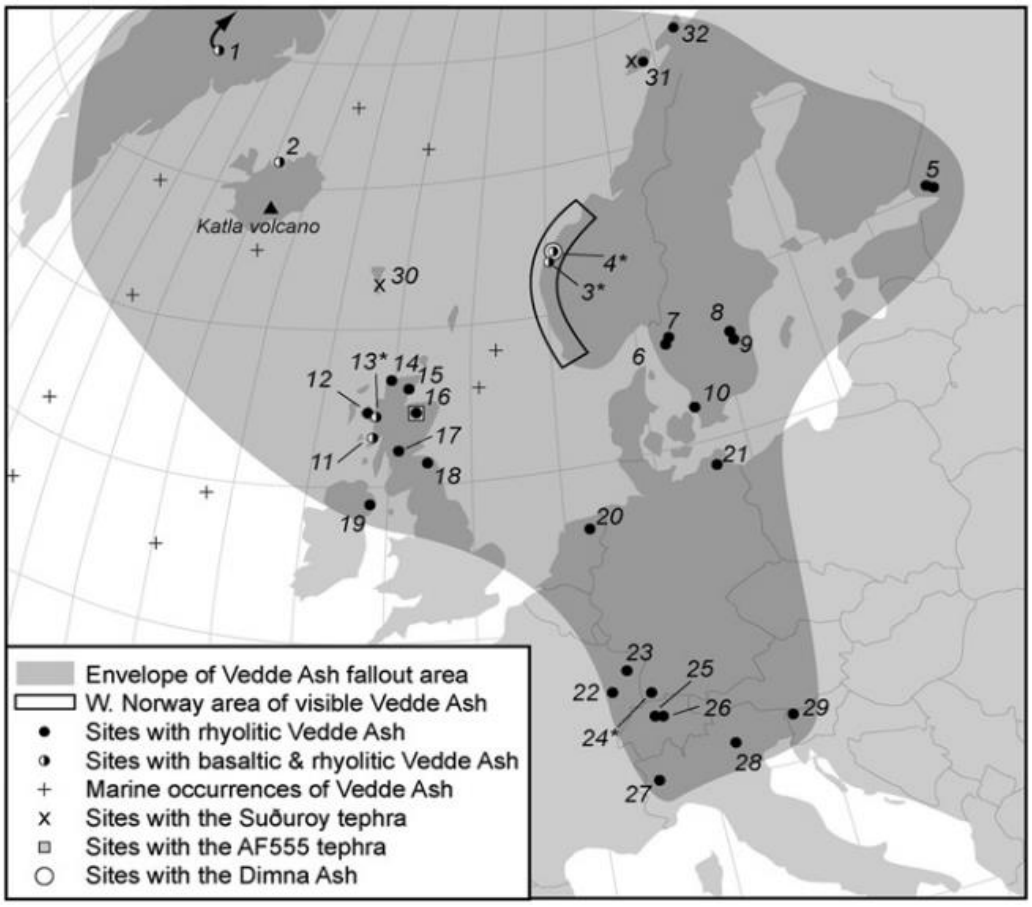

Fig. 3: *Map showing the distribution area of Vedde Ash as grey shaded area. Locations containing basaltic or rhyolitic Vedde Ash are shown, as well as locations containing one of the tephra's similar in composition to rhyolitic Vedde Ash. This map does not include the most recently (> 2012) discovered locations containing Vedde Ash. After Lane et al., 2012b.*

grey area highlights the estimated distribution fan of Vedde Ash based on these locations. Locations containing the geochemically similar AF555 tephra, Suðuroy tephra, and Dimna Ash are shown as well. Location 20 is Kostverloren Veen (Davies et al., 2005), more details on the numbering can be found in appendix A. According to this fan, Vedde Ash has reached the Netherlands and could therefore be present in the sediment record of Esmeer as well.

3. Pingos as study sites

When looking for far-travelled tephra in a sediment record, it is crucial to sample material from a proper study site. First of all, the site should be reached and affected by the distributed tephra material. Secondly, the site should be able to store such material in a traceable way. An example of a potentially suitable study site is a pingo remnant. This chapter contains general information regarding pingo development and specific information about the research location Esmeer, which is identified as a pingo remnant.

3.1 Pingo formation, collapse and infill

A pingo is a circular to oval hill formed by underground ice, of which the formation is limited to permafrost areas (Flemal, 1976). Pingos arise when water gets injected in the near-surface permafrost. Due to the low environmental temperatures, the underground water starts to freeze and forms a subsurface ice lens. Since water expands when freezing, the overlying soil will be pushed upwards, resulting in a hill in the permafrost landscape which is called a pingo.

Pingo collapse occurs due to various reasons. The underlying ice lens is pushing the overlying soil upwards, but this is limited by natural boundaries. Eventually, if the lens keeps growing, the overlying soil cannot completely cover the ice lens and tension fractures will arise in the overlying sediments. At these cracks, the ice lens is exposed to sunlight and will therefore start to melt. Exposure to sunlight can also occur after erosion of the overlying soil. Besides these physical processes, a rise in temperature caused by climate change will result in ice melting as well. When the ice lens starts to melt, the pingo will collapse and a circular depression will remain as a perennial landscape form, often surrounded by a rampart. These craterlike depressions will have a similar size as the original pingo. Since a pingo can reach relatively large sizes (up to a diameter of 1200 m, Holmes et al., 1966) its remaining depression can be of a significant size as well.

Since water stagnates in the lower parts of a landscape, lakes often emerge in the craterlike depression after pingo collapse. These lakes form relatively isolated systems since they are mainly controlled by airborne infill. The lake infill can consist of aeolian sediments and accumulated organic matter, consisting of pollen and vegetation originating from its direct surroundings. Windblown tephra can be deposited and preserved as well in such lakes. Due to

the limited and controlled infill of pingo remnants, tephra deposits like Vedde Ash and LST might be relatively easy to trace.

3.2 Esmeer

Esmeer is one of the numerous pingo remnants present in the Netherlands. Most pingo remnants occur in the northern provinces Friesland and Drenthe. In these areas the ground water pressure during the permafrost was sufficient to initiate the formation of an ice lens. The crater infill of the oldest pingo remnants are dated between 14 ka and 12 ka BP (de Gans, 2008).

Esmeer is located in the province of Drenthe in the north of the Netherlands (coordinates: N 53.006°; E 06.459°, see figure 4). It is a nearly circular lake with a diameter of circa 500 meters. With its depth of circa 13 meter, it is one of the deeper pingo remnants in the Netherlands. Since Esmeer is an isolated lake, its infill over the years is mainly controlled by airborne deposits, which enhances its potential to store and preserve airborne tephra. Considering its potential age it could have stored tephra deposited in the Lateglacial to Holocene period, including Vedde Ash and LST.

Figure 5 shows a satellite image of Esmeer and its direct surroundings. A rampart is present on the north-east side of Esmeer, which is typical for pingo remnants. The Esmeer sediment record is cored from the middle of the lake, as indicated by the red dot in figure 5.

***Fig 4**: Map of the Netherlands. The red dot indicates the location of lake Esmeer, Drenthe.*

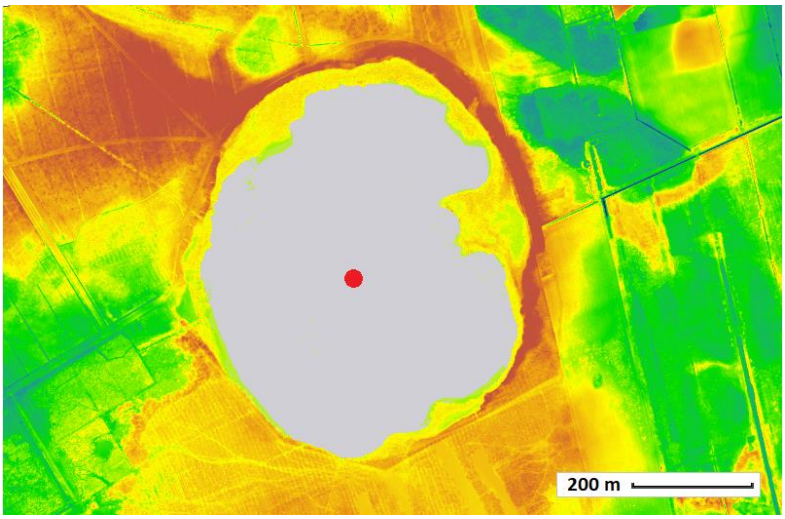

***Fig 5:** Elevation map of lake Esmeer. Height differences between low (blue) and high (red) are between 10-13 m asl. As indicated by the red rim, a rampart partly surrounds Esmeer. The red dot in the middle of the lake represents the coring location. After AHN.nl (AHN2 - maaiveld Blauw/Groen/Oranje, dynamische opmaak).*

4. Research strategy & techniques

In order to find tephra layers in the cores of Esmeer several research steps had to be conducted. The general research strategy starts with drilling sediment cores from an appropriate location where distal cryptotephra could have survived over thousands of years. As explained above, lake Esmeer is chosen for this. The sampled drilling cores must then be researched for the presence of tephra. By performing laboratory work including several separation techniques, potential tephra shards can be isolated from the drilling cores. If this is successfully executed, the isolated shards can be quantified to make a Tephra Shard Concentration (TSC). Furthermore, it needs to be confirmed that the observed shards are truly tephra shards. This can be done by determining the geochemical element concentrations of the encountered shards, for which additional laboratory work and geochemical analysis is required. The measured element concentrations of the shards can then be compared to determined Vedde Ash and LST element concentrations as measured by previous research.

The described general research strategy is applied in this research. This chapter contains an overview of all steps taken.

4.1 Sampling

Fieldwork was carried out in April 2013 by Timme Donders (Utrecht University) and colleagues. A sediment succession was cored from lake Esmeer by drilling into the sediments below the water surface. LOI (loss-on-ignition) was performed in January 2015 on the Lateglacial – Early Holocene record of the sediment record, named Esmeer B-II B3. This corresponds to a core depth of 415 to 504 cm. LOI is a method to obtain an objective lithological description of a sediment record by determining its organic content by ashing. Sub-samples of approximately 1 cm^3 each were taken at cm resolution. During LOI treatment the samples were weighed, dried for one night at 105°C, reweighed, burnt at 550°C for four hours and again reweighed (Heiri et al., 2001). All organic material is removed during this process, which is also useful for detecting tephra shards more easily. The remaining cored material was stored at a temperature of ± 7°C. The remaining material of each cubic centimetre subsample after LOI was labelled and stored for further analysis as well, which was carried out in this research.

Sub samples that could possibly contain Vedde Ash or LST were selected in January 2018. The LOI profile was used as a rough indication for the time period spanned by the sediment core, since intervals of low and high organic content are often associated with cold and warm intervals of the Lateglacial. So by comparing the LOI profile of lake Esmeer to those of other locations like Kostverloren Veen (Davies et al., 2005), it can function as a simple age-depth model and indicate at what depths tephra deposits could be present. Initially the depths 460 to 465 cm were selected

for finding Vedde Ash, and 484 to 488 cm for LST. A first search did not deliver convincing results and the search was broadened to the ranges 458 to 471 cm for Vedde Ash and 481 to 488 cm for LST.

4.2 Sample preparation prior to TSC

Finding cryptotephra deposits in a sediment record can be a demanding task since such deposits, consisting of small tephra shards in possibly low quantities, are invisible to the naked eye. To make this task as convenient as possible it is essential to isolate tephra shards from remaining sediment material. Blockley et al. (2005) suggested a laboratory procedure for the physical separation of distal glass shards from sediments, on which the procedure in this research was based. As explained in 2.1, tephra research is more valuable when similar methods are used in the research process. Therefore, the currently widely used procedure of Blockley et al. (2005) is used in this research as well. Figure 6 shows an overview of this procedure.

The steps needed to isolate tephra shards out of the source material were performed in the Geographical Laboratory at Utrecht University. The precise separation procedure to extract tephra shards from the subsamples of Esmeer differs slightly from the procedure suggested by Blockley et al., due to the availability of products in the laboratory and the characteristics of the source sediment. Step 1, selecting the subsamples, and step 2, LOI, were performed prior to this research and are described in 4.1 Sampling. The laboratory work started by putting the left-over material of LOI in labelled tubes and by lightly crushing it to loosen the cluttered material. Carbonates were removed as described in step 3 of Blockley et al. (2005) using 5% HCl instead of the prescribed 10% HCl. In step 4, the material was sieved using 200 µm and 30 µm sieves instead of the prescribed 25 µm and 80 µm sieves. For further geochemical analysis it was needed to see if tephra shards >30 µm were present in the Esmeer sample, since the laser beam size of the LA-ICP-MS is preferably circa 30 µm (see 4.6.2 for further explanation).

After sieving the samples, heavy liquid separation was applied to the 30-200 µm fraction to further segregate the sample material. Both LST and Vedde Ash have densities of 2.3-2.5 g cm^{-3}. Instead of using both 2.0 and 2.5 g cm^{-3} SPT to isolate the target material as suggested, only 2.5 g cm^{-3} SPT was used. Most material with a density smaller than 2.0 g cm^{-3} is organic material, which was already removed during LOI. The 2.5 g cm^{-3} SPT removes clastic material, leaving all material with densities < 2.5 g cm^{-3} including the target tephra in its float.

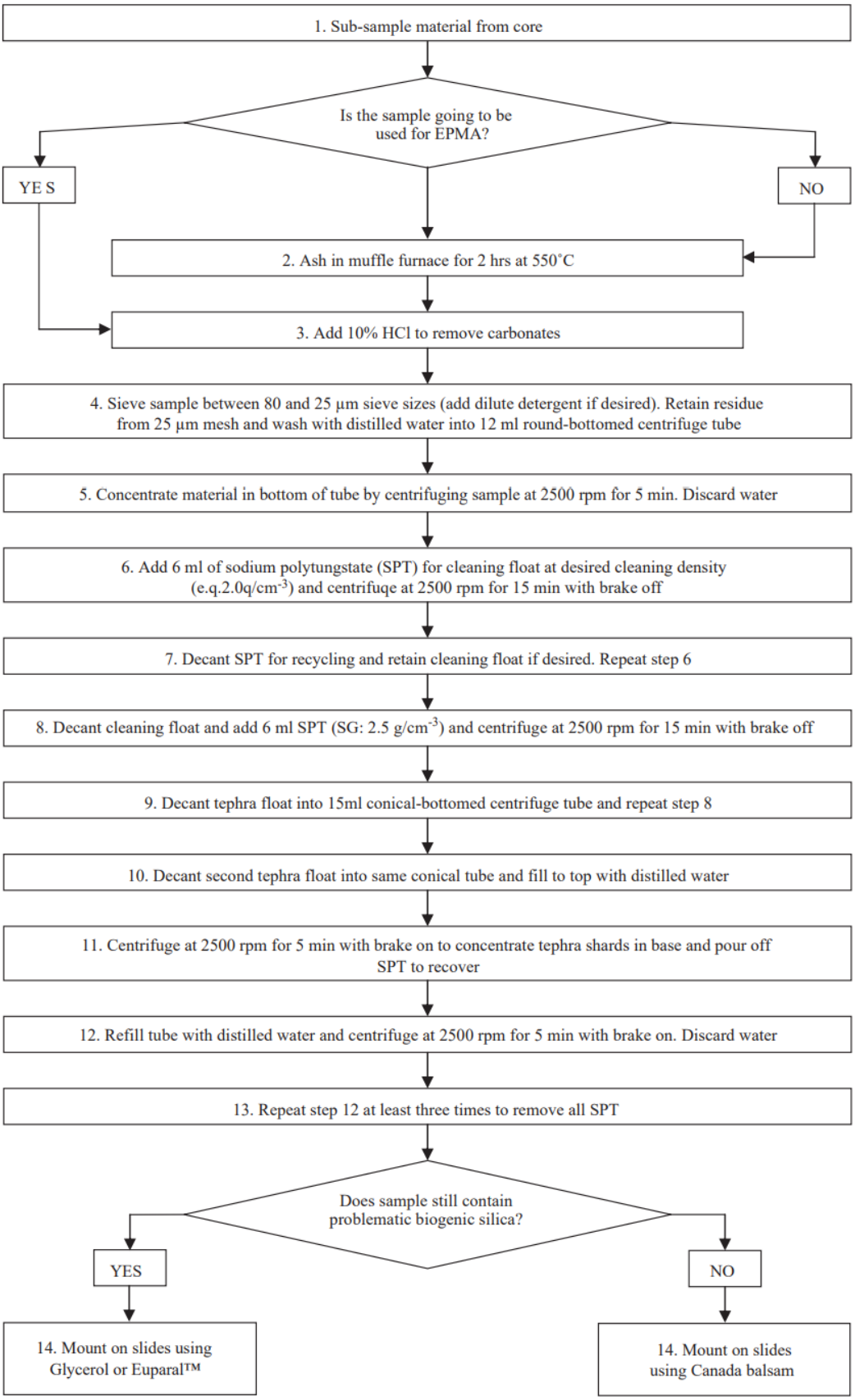

Fig 6: *Laboratory procedure to isolate tephra shards as suggested by Blockley et al., 2005.*

All sample material which was left over after the described steps was mounted on glass microscope slides. On each microscope slide one droplet of wet sample material was pipetted, which was then dried by placing the microscope slide on a hot plate at a temperature of 100°C. The dried material was mixed with a droplet of glycerine. A small cover glass is put on top and glued to the microscope slide using paraffin. All left over material was sampled, resulting in 6 to 15 microscope slides per cm^3 source sediment.

Prior to applying this method to samples from the sediment record of Esmeer, this method is tested using sediment samples from lake Hämelsee. This sediment record is previously researched and confirmed to contain several tephra layers, including Vedde Ash and Laacher See Tephra (Jones et al., 2018).

4.3 Tephra Shard Concentration

A Tephra Shard Concentration (TSC) diagram is made per centimetre depth of the sediment core for both the Vedde Ash and Laacher See Tephra target depths. This involves recognizing and counting all individual shards by the use of an optical microscope at xx magnification. To get familiar with the morphology of tephra shards, microscope slides containing tephra shards from lake Hämelsee are studied prior to counting possible tephra shards in the sediment record of Esmeer.

For the quantification of Vedde Ash and Laacher See Tephra an optical Leitz Wetzler microscope was used. A representative number of all microscope slides was counted in a systematic way to make sure each single grain on the slide was visible under the microscope during the counting process. The total number of shards per cm depth was obtained by normalising the number of shards of the counted microscope glasses to the total amount of microscope glasses.

4.4 Sample preparation prior to geochemical analysis

To confirm whether the observed and counted shards are truly tephra shards, their element concentrations should be measured by geochemical analysis. To perform such geochemical analysis, additional sample preparation involving laboratory work is required. For a reliable correlation to tephra deposits it is crucial that the geochemical composition of glass shards remains unaltered by any laboratory analytical procedures (Blockley et al., 2005). Therefore LOI (as used in the previously described lab procedure in 4.2) cannot be used and new laboratory work was needed for sample preparation.

Fresh sub-samples were taken from the drilled material of Esmeer core (sample Esmeer B-II B3) which had been has been kept well wrapped in the cold storage at 5 degrees. The depths of these fresh subsamples were based on the results of the Tephra Shard Counts. For Vedde Ash, the

depths 468-469 cm and 469-470 cm contained a large peak in potential tephra shards, therefore subsamples of circa 3 cm^3 were selected from these depths. The TSCs of the LST were less conclusive (see 5.1.2), yet sub-samples of circa 3 cm^3 were selected from the depths 485-486 cm and 486-487 cm.

Again, the procedure of Blockley et al. (2005) was used as a guideline for sample preparation, although some alterations were made due to the availability of lab material and the characteristics of the material. First, about 20 mL 5% HCl is added to remove carbonates overnight. Then, instead of applying LOI, hydrogen peroxide (H_2O_2) is used to remove organic material. The samples were put in a mixture of 40 mL distilled water and 30 mL of 30% hydrogen peroxide, resulting in a liquid of circa 13% hydrogen peroxide. The samples were in this mixture for two nights since the samples seemed to react quite slowly. All sample material was sieved using sieves of 8 µm and 200 µm. Material < 8 µm is washed away and all material > 200 µm is stored for potential further analysis. Heavy liquid separation is used again to further segregate the samples. Instead of using only 2.5 gcm^{-3} SPT as was done in the previous described lab work, SPT of densities 2.0 g cm^{-3}, 2.3 g cm^{-3} , and 2.5 gcm^{-3} is used. 2.0 g cm^{-3} SPT will separate any leftover organic material which has not been removed by the treatment of hydrogen peroxide. By using 2.3 g cm^{-3} SPT as well, the sample material will be more precisely divided, making it easier to detect tephra shards in the target density. After these steps, it was necessary to dry the sample material in order to have loose tephra shards instead of cluttered ones. Therefore a layer of 90% ethanol was added to the sample, which evaporates at room temperature and leaves a dry and loose sample.

The dry, left-over material was spread over a petri dish and individual tephra shards were picked using a thin needle and a microscope. The individual handpicked tephra shards were placed on double-sided tape on a mount. A total of ten mounts were made: two mounts of depth 468-469 cm (Vedde Ash), four mounts of depth 469-470 cm (Vedde Ash), two mounts of depth 485-486 cm (LST), and two mounts of depth 486-487 cm (LST).

The ten above described mounts were further processed in the grindery of Utrecht University. The mounts were covered by a cm-thick layer of epoxy that solidified overnight. The mounts were grinded until the glass shards became exposed and showed a fresh surface. Due to the fact that the handpicked glass shards were small and thin, the mounts had be grinded and polished with great care. Despite these efforts, the shards of two Vedde Ash mounts were grinded away and could therefore not be used for geochemical analysis. On the other eight mounts up to five particles surfaced after grinding. Despite the fact that some mounts contained more shards than the exposed ones, the mounts were not grinded further since the exposed shards would get grinded away. All eight mounts were coated by a thin layer of carbon in preparation for geochemical analysis.

4.5 Major and minor element concentration (EPMA)

Electron Probe Micro Analysis (EPMA) is a well-known technique for establishing major and minor element concentrations. An Electron Probe Micro Analyser is a microbeam instrument that is primarily used for non-destructive and in situ chemical analysis of solid samples. It delivers a precise and quantitative major and minor elemental 'fingerprint'. This technique can be used for volcanic glass shards as well, first described by Smith and Westgate (1968).

Two different EPMA methods are used in this research: WDS (wavelength-dispersive spectrometer) for quantitative analysis of eleven major and minor elements and SE (Secondary Electrons) for creating detailed maps of each sample. This chapter describes both techniques and details on the measurement settings.

4.5.1 Wavelength-dispersive spectrometer (WDS)

WDS is an analytical technique using characteristic X-rays to determine the composition of the sample of interest. A electron beam of sufficient energy is accelerated in the electron column of the EPMA. Once this electron beam hits the sample, the electrons start to interact with the sample. Amongst others, X-rays with different wavelengths are generated. The wavelength of these X-rays are characteristic for the element that generated them. All generated X-rays with different wavelengths reach a crystal. The crystal structure can be regarded as lattice planes separated by the interplanar distance *d*, and only reflects X-rays that satisfy Bragg's Law (see equation 1).

$$2\mathrm{d}\sin\theta = n\lambda$$

Eq 1: *Bragg's Law, where* d *is the interplanar distance,* θ *is the angle between the incident wave and the lattice plane,* n *is a positive integer and λ the wavelength of the incident wave.*

As a result of this, only a single wavelength is sent into the detector. By changing the position of this crystal relative to the sample, different X-ray wavelengths will satisfy Bragg's law and can be sent into the detector. Consequently, only one element can be measured per detector at a time and the analytical crystal must be moved during a single measurement. EPMA will then translate the received X-ray signal into a major and minor element concentration.

4.5.2 Secondary Electron (SE) imaging

Besides WDS, another method is used: Secondary Electrons (SE). SE imaging provides information of the topography or morphology of a sample. Just as in WDS measurements, an electron beam of sufficient energy is accelerated. When this electron beam hits the sample, atoms of the sample

get excited and generate secondary electrons from the surface of sub-surface of the sample. The number of secondary electrons emitted depends on the topography of the sample. A detector counts the number of incoming secondary electrons, and based on these numbers a well-defined image of the topography is created. These SE images can function as detailed mount maps, which is useful for navigating during the LA-ICP-MS measurements.

4.5.3 EPMA measurement settings & details

EPMA measurement were performed using the JEOL JXA-8530F Electron Probe Micro Analyzer at the GeoLab, Utrecht University. This EPMA is provided with five spectrometers, so five elements could be measured at the same time.

The eleven elements measured during WDS were: Si, Ti, K, Na, Fe, P, Cr, Ca, Mg, Mn, and Al (in this particular order in batches up to five elements). Since sodium is a volatile element and tends to get lost during measurements, this element was included in the first five elements to be measured. The beam current was 10 nA with a voltage of 15kV. The spot size varied between 3 to 5 µm, depending on the size of the shards. In total, 37 WDS-EPMA measurements were performed on 14 different tephra shards, per tephra shard 1 to 4 measurements were taken. Prior to these measurements, a diopside standard was measured to check whether the EPMA performed correctly.

4.6 Trace element concentrations (LA-ICP-MS)

In some cases the major and minor element fingerprint may not be conclusive in correlating tephra shards to their source volcanic eruption (Tomlinson et al., 2010). Many evolved magmas are compositionally similar in major and minor elements, especially those erupted from the same volcano. The abundances of trace elements (concentration typically <100 ppm) in magmas are more affected by magmatic processes than major element concentrations, thus resulting in a wider variability of trace elements compared to major elements (Allan et al., 2008). An example of such a magmatic process is fractional crystallization, which significantly affects trace element concentrations but has only a very limited influence on major element compositions. In summary: by analysing the trace element fingerprint of tephra shards as well, more precise tephra correlations can potentially be established than by using the major and minor element concentration alone. Therefore, the results of the EPMA analysis of this research are complemented by trace element analysis.

A method to establish the trace element concentration is the analytical technology Laser Ablation Inductively Coupled Plasma Mass Spectrometry (LA-ICP-MS). LA-ICP-MS is a destructive method, able to detect and quantify trace elements that typically have a low concentration rate (1 ppb-

100 ppm). Largely because of the speed and the relatively low costs of analysis, LA-ICP-MS has developed over the last year into the most widely used trace element technique in tephra studies (Pearce, 2014). It enables highly sensitive elemental and isotopic analysis performed directly on solid samples. This chapter contains an overview of the general working of LA-ICP-MS, the details of this research' measurements, and the required data processing.

4.6.1 LA-ICP-MS

A measurement performed by LA-ICP-MS consists of multiple steps. First, a laser beam is focused on the sample surface that hits the sample. This laser locally destroys the sample by generating fine particles out of it. This process is known as Laser Ablation (LA) and leaves a crater in the sample, of which the size depends on the laser spot size. The ablated particles are transported in a stream of inert gas directly into the argon plasma of the ICP-MS. The ICP source converts the atoms of the elements to ions (ionization). The ions from the plasma are extracted into the mass spectrometer where they are separated on the basis of their mass-to-charge ratio. A detector receives an ion signal proportional to the concentration, resulting in counts per second per element of interest.

This analytic tool is known as a semi-quantitative method, it simply counts the amount of elements of interest. These raw data are often further processed into concentrations for further analysis. This can be done by calibration using homogeneous standards of which the chemical composition is well established. By linking counts per second to established concentrations, LA-ICP-MS data can be further processed into concentrations (ppm) rather than only using counts per second.

4.6.2 LA-ICP-MS measurement settings & details

To give insight in how all LA-ICP-MS measurements are performed, this section will give details on the measurement setting and details.

The pulse energy during measurements was 8.8 J cm^{-2} and the pulse repetition rate was 5 Hz for most measurements. Initially the more common repetition rate of 10 Hz was used, but after the first measurement this was adapted to 5 Hz because of the thinness of the glass shards. If the repetition rate is relatively high, the laser will penetrate the thin shards in a very limited amount of time. Lowering the repetition rate will cause a less intense measurement and yield a longer usable measurement time. Each measurement had a total duration of circa 2 minutes. The first minute was a background measurement and the second minute was the actual measurement during which the laser ablated the spot of interest. The spot size of the laser varied between 10 and 30 µm during the measurements, and was depending on the size of the glass shards. A larger laser spot results in a higher yield of ablated material, which enhances the reliability of a

measurement. In some cases the laser spot may have covered the surrounding epoxy material as well, resulting in epoxy being ablated and measured as well along with tephra material. An extra measurement was performed on the epoxy material which did not show any presence of trace elements. Therefore it is likely that any ablated and measured epoxy did not influence the trace element concentration of the measured shards. In total, 25 measurements were performed in 16 tephra shards, so it was possible to measure 9 shards twice. Executing more than 2 measurements per shard was impossible due to the small size of the tephra shards and the preferred laser spot size of 30 or 20 µm .

To check whether the LA-ICP-MS was performing correctly during the measurements, the standard BCR2G was used. BCR2G is a basaltic volcanic class that was measured after every five glass shards measurements. The BCR2G measurements did not show any significant deviations, therefore it could be assumed that LA-ICP-MS was performing correctly.

4.6.3 LA-ICP-MS data processing

LA-ICP-MS is a semi-quantitative method because the counts measured by the mass spectrometry must be converted into the actual concentration of trace elements. This can be done by calibration using certified reference standards. In this research, the Nist standard N612 was used, a homogeneous silicate glass of which the composition is well established. Calibration was done by assigning the known quantities of trace element in N612 to the measured counts of the mass spectrometry.

The measurements of LA-ICP-MS were further processed using the program GLITTER, version 4.4.3. One of the features of this program is visualising trace element measurements by showing counts per second graph for individual elements. These graphs were used to select a stable range of each measurement that could be used for determining the trace element concentration. A stable range is defined as a consistent range with fairly constant values lacking peaks and not significantly sloping down in the counts per second graph. The vast majority of the measurements showed such a pattern, but only for a limited period of time. Since the mounted glass shards was typically very thin, the laser easily penetrated the material after which it started measuring the surrounding epoxy. A test measurement revealed that the surrounding epoxy does not contain trace element material. So in most measurements, the difference between measuring a glass shard or its underlying epoxy was clear by a significant drop in measurement signal. The selected ranges in GLITTER on which the trace element concentrations were based, varied between 3 to 28 seconds (or 6 to 28 seconds for the accepted measurements, see 5.3). The quality of the measurement and therefore the length of the range can be depending on the positioning of the glass shard, the repetition rate, the laser spot size, and impurities on the glass shards. GLITTER also produced a 1σ error calculation for each single trace element measurement.

4.7 Chronological context

Once a layer of tephra is found and geochemically analysed, it can be placed in a broader LiChronological context. As earlier described, an LOI profile can function as a simple age-depth model. It furthermore contains information about the lithology of the sediment record of Esmeer, which is describes as a mixture of gyttja, sand and clay (Zwier, master thesis, 2018). An LOI profile indicates the relative amount of organic material and non-organic material and therefore reveals a clue of the environment of Esmeer at the time of shard deposit.

Besides the LOI profile, a detailed pollen diagram can also be used to place the tephra deposits in an environmental context. A pollen analysis has recently been made by Maaike Zwier (master thesis, 2018). Samples for pollen analysis were taken every 2 to 4 cm, this would account for circa one sample every 140 yr. After counting pollen in the initial set of samples, the resolution was increased at the zone boundaries to improve the zone boundary positions. The pollen characteristics (both amount and type) can often be associated to certain time periods. So not only does this pollen diagram provide information about the environment during glass shards deposits, it also functions as another rough age-depth diagram. The identified periods based on the pollen analysis are visible in table 1. The detailed pollen diagram of lake Esmeer is added in appendix B.

Zone	Section	Core depth (cm)	Period
I	b	504 - 499	Bølling
I	c	499 - 496	Earliest Dryas
II	a	496 - 485.5	Allerød - *Betula* phase
II	b	485.5 - 481	Allerød - *Pinus* phase
III	a	481 - 474	Younger Dryas
III	b	474 - 462.5	Younger Dryas - *Empetrum* phase
IV		462.5 - 456	Preboreal
V		456 - 445	Boreal

Table 1: *Zones identified in sediment record of Esmeer, based on pollen analysis. After Zwier (master thesis, 2018).*

5. Results

5.1 Shard morphology & concentration

More than 100 microscope slides containing all left-over material after separation techniques are studied for the presence of volcanic glass shards. This section contains an overview of the results obtained after intensively examining these microscope slides, originating from both the target

depths for Vedde Ash and LST. This includes a shard morphology description and an estimated concentrations based on the number of shards present in the studied microscope slides.

5.1.1 Shard morphology and concentration at Vedde Ash depth

During intensively searching the microscope slides possibly containing Vedde Ash shards, one particular type of material was notably different from any other material present in the sample. It can be described as sharply edged with a glassy appearance (see figure 8). The shapes vary from flat and platy to three dimensional constructions. The latter include elongated shaped shards that have three 'wings', as visible in the third row and fourth row (middle and right picture) of figure 8. The observed shards turned black at crossed polarized light (XPL), which is an indication for glass (since glass is an isotropic material, which generally turns black at XPL). The colours of these shards varied from colourless and transparent to pale green and pale pink. These colourings were likely to be a result from burning (oxidation of minerals) during the LOI. The fresh shards all appeared transparent and colourless.

TSC table

Depth (cm)	Concentration (shards cm^{-3})
458-459	44
459-460	39
460-461	45
461-462	47
462-463	56
463-464	83
464-465	71
465-466	85
466-467	81
467-468	125
468-469	186
469-470	221
470-471	37

Table 2: *Counted glass shards per cm^3 material at potential Vedde Ash depths.*

TSC diagram

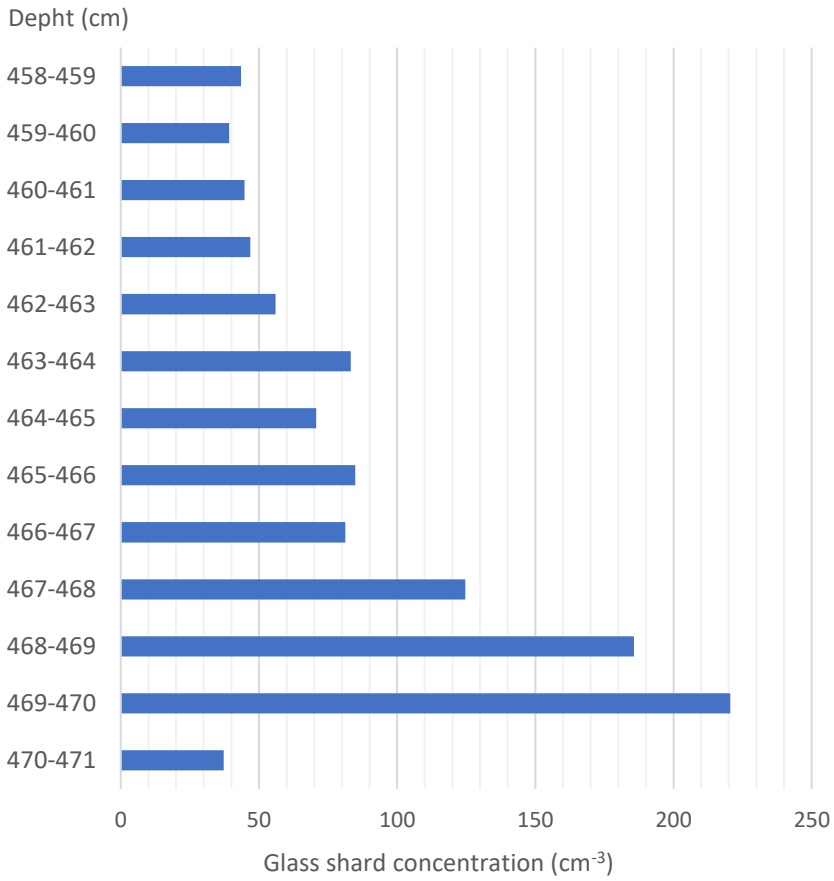

Fig. 7: *Glass shard concentration at potential Vedde Ash depth.*

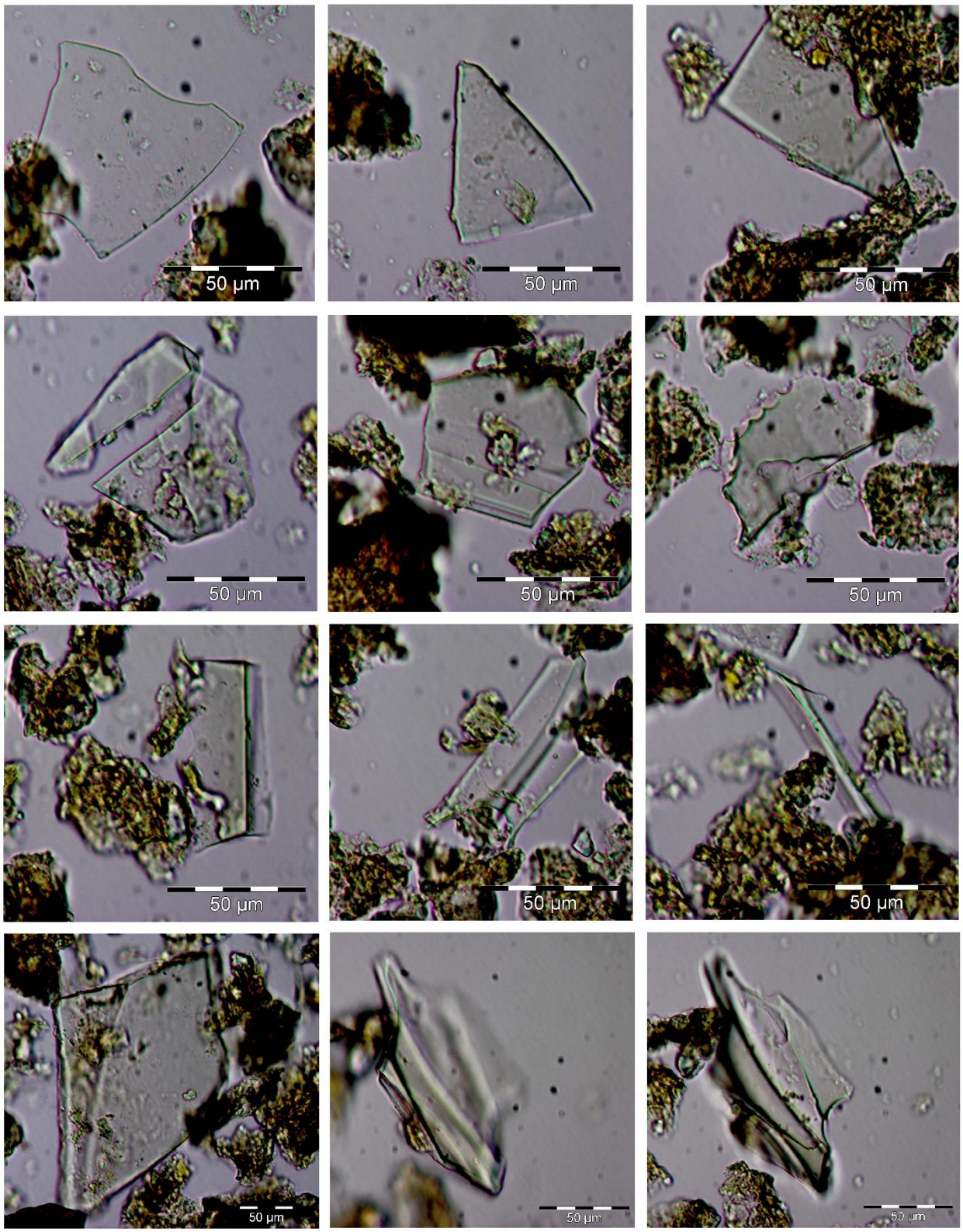

Fig. 8: *Shards from depth 468-470 cm (after LOI treatment) with various shapes, angularity, thickness and size. The lowest row contains larger shards, note the difference in 50 µm scale bar. The last two pictures are of the same shard but token at various zooming level to indicate the three dimensional shape.*

Due to the shape and optical characteristics, this material was identified as glass. By systematically counting the amounts of such glass shards present per centimetre depth, a Tephra Shard Concentration (TSC, number of tephra per cm^3 source material) is made. The results of this counting process for the target depth for Vedde Ash (458-471 cm) are visible in table 2. The TSC diagram (figure 7) shows an almost classic tephra distribution. At 469-470 cm depth, the amount of shards suddenly increase to a maximum value of 221 shards per cm^3 (in the fraction 30-200 µm). Above this basal peak, the amount of glass shards gradually decrease to a minimum value of 37 glass shards per cm^3. The combination of this type of distribution, the particular depth at which the shards are found, and the morphology of the glass shards are a strong indication for the presence of tephra, particularly Vedde Ash.

For further geochemical analysis new fresh subsamples were taken at depths 468-469 cm and 469-470 cm since these peaks contained the largest amounts of shards.

5.1.2 Shard morphology and concentration at LST depth

In contrast to the microscope slides from Vedde Ash depth, the slides at LST depth (481-488 cm) contained little glass like material. Some shards were observed that were sharply edged and varied in colour from colourless to pale green and pink (see figure 9). These shards were significantly lower in amount, as shown in the TSC table (table 3) and the TSC diagram (figure 9).

The TSC diagram (figure 10) shows a maximum peak of 37 shards per cm^3 at 486-487 cm depth. This could point to presence of LST at that depth. However, the low amount of glass shards should be taken into serious consideration since the human error of particles mistakenly counted as glass shards will be of more influence. At all counted depths (for both Vedde Ash and LST), a minimum of 15 shards is observed. Either there are glass shards present in all depths, or there is a human error of at least this magnitude.

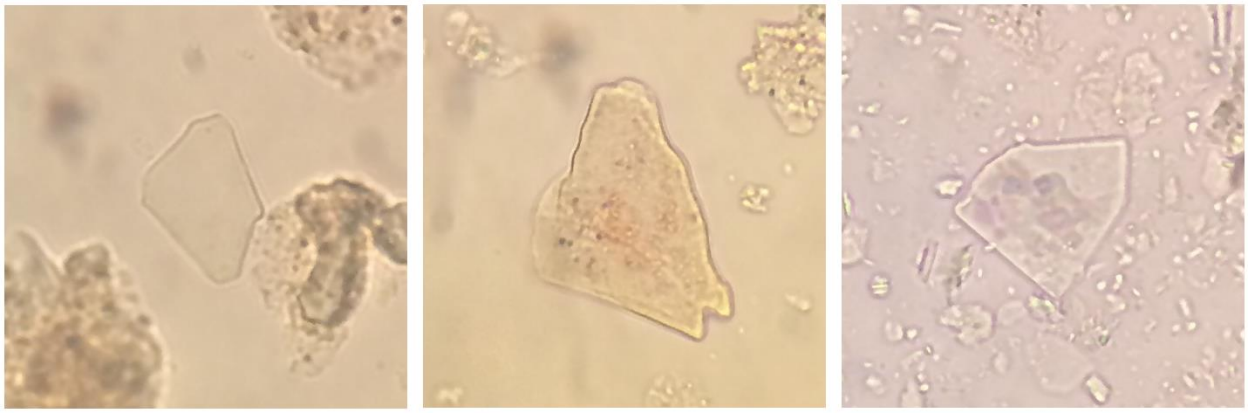

Fig 9: *Shards at LST target depths. No precise scale bar is available, the sizes of the shards is between 30 and 200 µm.*

TSC table

Depth (cm)	Amount
481-482	15
482-483	22
483-484	24
484-485	26
485-486	19
486-487	37
487-488	20

Table 3: *Counted glass shards per cm³ material at potential LST depths.*

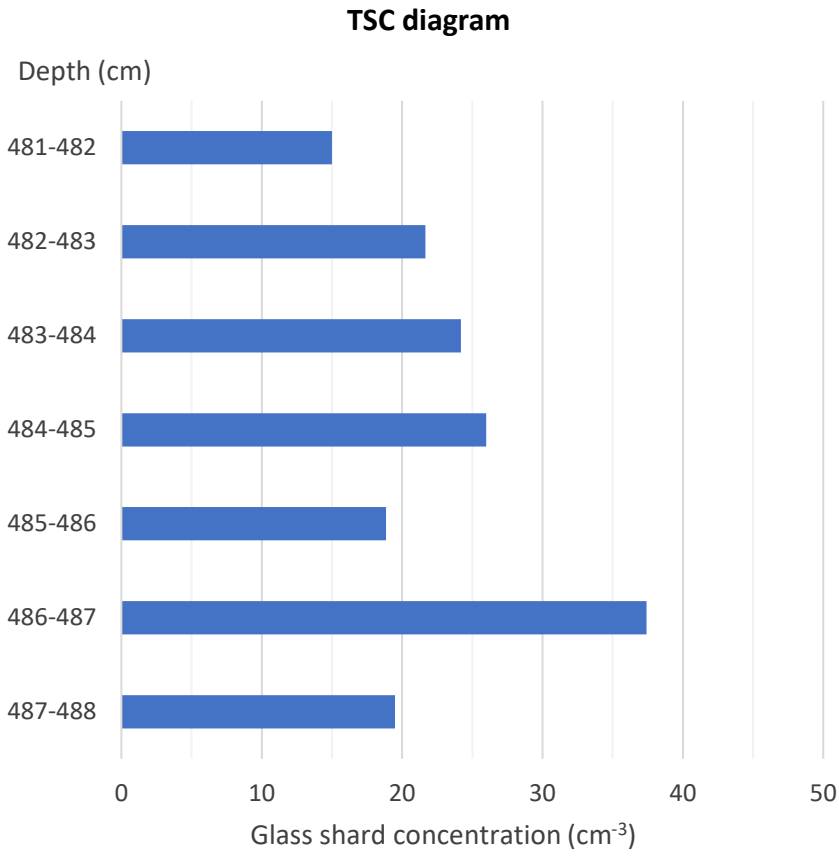

Fig 10: *Glass shard concentration at potential LST depth.*

Although strong indication of the presence of LST is lacking, new fresh subsamples of depths 485-486 cm and 486-487 were taken for further geochemical analysis. Considering the peak in figure 10, depth 486-487 cm is the most obvious choice for this. LST is often found as a single peak within the sediment record, sometimes accompanied by a second, adjacent peak as well. Therefore, an adjacent depth (485-486 cm) is chosen as well to broaden the search for LST, although strong evidence of LST depth is missing for this particular depth.

5.2 Major and minor element concentration (EPMA)

Prior to geochemical analysis by both EPMA and LA-ICP-MS, the new fresh subsamples of depths 468-470 (Vedde Ash) and 485-487 cm (LST) were treated in laboratories to create measurable mounts (explained in section 4.3.1). Eight mounts were available for EPMA measurements, of which four contained potential Vedde Ash shards, and four contained potential LST shards. The LST mounts contained only one to three exposed shards per mount, whereas the Vedde Ash mounts contained up to five exposed shards. Table 4 shows an overview of all measurable

mounts. The amount of shards is based on the shards visible and therefore surfacing during EPMA measurements. As visible in table 4, on mount 8 no shards appeared to be surfaced during the grinding process.

Mount	Depth in core (cm)	Target tephra	Number of shards
1	469-470	Vedde Ash	5
2	469-470	Vedde Ash	2
3	469-470	Vedde Ash	3
4	469-470	Vedde Ash	5
5	485-486	LST	2
6	485-486	LST	1
7	486-487	LST	2
8	486-487	LST	0

Table 4: *Overview of mounts, the depth of which the shards originate, the corresponding target tephra, and the amount of measurable shards present on this mount.*

5.2.1 Laacher See Tephra EPMA

Four mounts (5-8) were available for EPMA measurements, of which mount 8 did not show any surfaced shards. Mount 5 contained two measurable shards, but this was different for mount 6 and mount 7. Both of these mounts showed shards which were apparently placed upright in the mount instead of flat, leading to a section too small to measure. For WDS-EPMA measurements, a certain interaction volume is needed to perform a proper measurement. This volume would exceed the volume of the shard, leading to unreliable measurements. The only reliable measurements could therefore be delivered by mount 5, of which the results are visible in table 5. This table shows the weight percentages of eleven major and minor elements as oxides and the total amount of measured weight percentage.

mount	SiO_2	TiO_2	Al_2O_3	FeO	MnO	MgO	CaO	Na_2O	K_2O	P_2O_5	Cr_2O_3	TOTAL	spot size (µm)
5	44.48	0.76	26.03	7.45	0.06	1.39	0.32	0.14	4.67	-0.05	0.01	85.27	4
5	43.05	0.35	32.70	1.25	0.02	0.80	0.08	0.69	9.09	-0.06	0.05	88.02	4
LST	56-61	0.1-0.6	20-23	1-3	0.1-0.5	0.0-0.4	0.3-2	7-12	5-8	-	-	-	-

Table 5: *WDS-EPMA results of major and minor element concentration of shards at LST depth. All oxides are in weight percentages (wt%). Lowest row contains the general major and minor element concentration of LST, based on Bogaard and Schminke (1984) and Tephrabase.org.*

Both measurements show a relative low amount of total measured weight percentage (only up to 88.02%) which decreases their reliability. This might be caused due to an unknown water concent in the measured shard, since H is too light to be detected by EPMa The LST characterisation does not resemble the measurements in table 5. Even if the measured values are adjusted by normalisation to a total of 100 wt%, both measurements do not fall within the range characterizing LST. Because of the low amount of measurements (two), the poor quality of the measurement (wt% only up to 88.02) and the mutual deviating weight percentages, it is unlikely that these shards can be correlated to LST. Therefore these shards are not further measured by LA-ICP-MS.

5.2.2 Vedde Ash EPMA

For WDS-EPMA measurements of potential Vedde Ash shards, four mounts were available originating from 469-470 cm core depth. All mounts contained multiple surfacing shards that could be measured. The results of the WDS-EPMA measurements are visible in table 6. This table shows the weight percentages of eleven major and minor elements as oxides, the total amount of measured weight percentage as well as the spot size. The underscores in table 6 mark which measurements originate from the same glass shard, since the majority of the glass shards were measured multiple times. This gives an insight in either the quality of the measurements, or the (non-)homogenenous element concentration of a glass shard.

In total, 37 measurements were taken of which six are rejected, visible in table 6 under *rejected data*. These data are rejected for two reasons. Measurements 1.1, 1.2, and 1.3 have a low amount of total measured weight percentage and are therefore considered as less reliable. Measurements 1.4 and 1.5 are rejected for a different reason. Appendix C contains a table showing the error percentage per element and per measurement. The element error percentage of most measurements is quite consistent, but measurement 1.4 and 1.5 show deviating error percentages for elements Ti, Ca, Mg, Fe, Mn, and Al. These two measurements are therefore rejected as well. Measurement 2.1 is rejected because of its high error percentage of Na.

The majority of the accepted measurements show consistent weight percentage values for both the individual oxides as well as the total amount of weight percentages. To visualise this consistency in weight percentage, all results of are plotted in figure 11, showing all individual EPMA measurements as weight percentage per oxide (excluding the six rejected measurements). The largest variation is seen in wt% of SiO_2, which makes sense since this is the element with the highest wt%. Another notable variation is seen in Na_2O wt%. This cannot be explained by a natural variation due to the large wt% of Na_2O, since this is only 4.05 on average.

	SiO_2	TiO_2	Al_2O_3	FeO	MnO	MgO	CaO	Na_2O	K_2O	P_2O_5	Cr_2O_3	TOTAL	spot size (µm)
1.6	71.12	0.27	13.33	3.85	0.13	0.18	1.34	5.00	3.41	0.00	-0.01	98.61	5
1.7	70.84	0.26	13.24	3.83	0.18	0.22	1.34	2.46	3.10	-0.01	-0.01	95.45	5
1.8	68.59	0.29	13.02	3.57	0.15	0.20	1.27	3.73	3.17	0.02	0.00	94.02	5
1.9	67.82	0.27	12.88	3.75	0.13	0.21	1.25	3.87	3.15	0.00	0.02	93.34	5
2.2	68.30	0.26	12.93	3.85	0.14	0.22	1.29	3.76	3.27	-0.01	0.02	94.02	3
2.3	70.86	0.30	13.35	3.78	0.15	0.20	1.20	4.06	3.33	0.00	-0.02	97.21	3
2.4	71.17	0.29	13.13	3.87	0.18	0.20	1.31	2.18	3.10	0.01	-0.04	95.41	4
2.5	70.20	0.29	13.10	3.78	0.16	0.20	1.29	2.03	2.91	0.00	0.00	93.95	4
3.1	70.31	0.25	13.21	3.95	0.14	0.23	1.26	4.36	3.23	0.01	0.01	96.96	5
3.2	70.33	0.26	13.15	3.82	0.16	0.20	1.27	4.58	3.24	-0.03	0.01	96.98	5
3.3	70.18	0.26	13.23	3.75	0.15	0.19	1.26	4.52	3.30	0.01	0.00	96.86	5
3.4	70.54	0.28	13.40	3.81	0.11	0.21	1.28	4.63	3.27	0.02	0.02	97.56	5
3.5	69.14	0.25	12.95	3.73	0.17	0.21	1.31	4.51	3.27	0.02	-0.02	95.52	5
3.6	69.66	0.28	13.07	3.81	0.15	0.22	1.32	4.54	3.28	-0.03	0.03	96.33	5
3.7	69.03	0.25	13.13	3.71	0.12	0.22	1.29	4.52	3.25	-0.01	-0.02	95.51	5
3.8	70.26	0.27	13.62	3.78	0.14	0.20	1.27	3.86	3.24	0.04	-0.03	96.65	3
3.9	68.83	0.26	12.84	3.74	0.16	0.21	1.28	3.31	3.20	0.07	-0.02	93.88	3
3.1	70.01	0.30	13.03	3.68	0.14	0.20	1.26	3.33	3.19	-0.01	0.02	95.15	3
4.1	68.87	0.27	12.78	3.81	0.20	0.19	1.29	4.81	3.37	0.03	-0.01	95.61	5
4.2	68.23	0.28	12.79	3.77	0.14	0.20	1.31	4.91	3.29	-0.01	-0.04	94.88	5
4.3	69.57	0.29	12.95	3.68	0.13	0.22	1.28	4.41	3.34	0.01	0.01	95.89	5
4.4	69.69	0.25	13.11	3.98	0.18	0.18	1.28	2.75	3.13	-0.03	-0.02	94.51	5
4.5	68.41	0.25	12.85	3.64	0.15	0.19	1.27	4.33	3.16	0.01	-0.05	94.21	5
4.6	68.76	0.25	13.05	3.77	0.14	0.20	1.25	4.68	3.21	-0.03	-0.03	95.27	5
4.7	68.90	0.30	12.81	3.77	0.18	0.20	1.32	4.88	3.36	0.00	-0.01	95.70	5
4.8	68.74	0.25	12.66	3.74	0.14	0.18	1.31	4.79	3.35	-0.01	-0.02	95.15	5
4.9	69.19	0.32	13.09	3.72	0.18	0.21	1.30	4.67	3.32	0.01	-0.02	95.99	5
4.1	69.41	0.27	13.32	3.65	0.14	0.20	1.23	3.73	3.18	0.00	-0.04	95.10	5
4.1	70.27	0.28	13.30	3.61	0.15	0.18	1.25	4.10	3.27	-0.06	-0.01	96.34	5
4.1	70.49	0.28	13.58	3.84	0.18	0.21	1.34	4.28	3.29	-0.05	0.02	97.46	5
4.1	69.50	0.29	13.37	3.73	0.15	0.18	1.23	3.88	3.23	0.02	0.00	95.57	5
mean	69.67	0.27	13.11	3.77	0.15	0.20	1.28	4.05	3.23	0.00	-0.01	95.65	
1σ	1.02	0.02	0.23	0.09	0.02	0.01	0.03	0.80	0.11	0.03	0.02	1.23	
rejected data													
1.1	64.74	0.27	11.80	3.61	0.16	0.21	1.21	3.84	2.95	-0.01	-0.02	88.76	4
1.2	57.34	0.23	9.75	3.23	0.16	0.16	1.08	2.95	2.70	0.01	0.01	77.61	4
1.3	55.15	0.24	9.81	3.21	0.08	0.14	1.03	2.02	2.65	0.02	-0.01	74.33	4
1.4	74.11	0.11	11.30	2.09	0.06	0.00	0.65	3.41	2.99	-0.07	-0.01	94.63	4
1.5	73.35	0.13	11.19	2.11	0.07	0.01	0.67	3.32	3.02	-0.05	0.00	93.84	4
2.1	72.30	0.29	13.15	3.92	0.15	0.21	1.35	1.35	3.00	-0.01	-0.02	95.68	3
VA	68-72	0.2-0.4	12.5-13.7	3.4-4.2	0.1-0.2	0.2-0.3	1.0-1.7	4.5-5.0	3.0-3.7	-	-	-	

Table 6*: Major and minor element concentration in wt% as measured by WDS-EPMA. The underscores in the left column mark which measurements are performed on the same shard. The lowest line contains a Vedde Ash characterisation (after Mangerud et al., 1984; Blockley et al., 2007 and Lane et al., 2012b)*

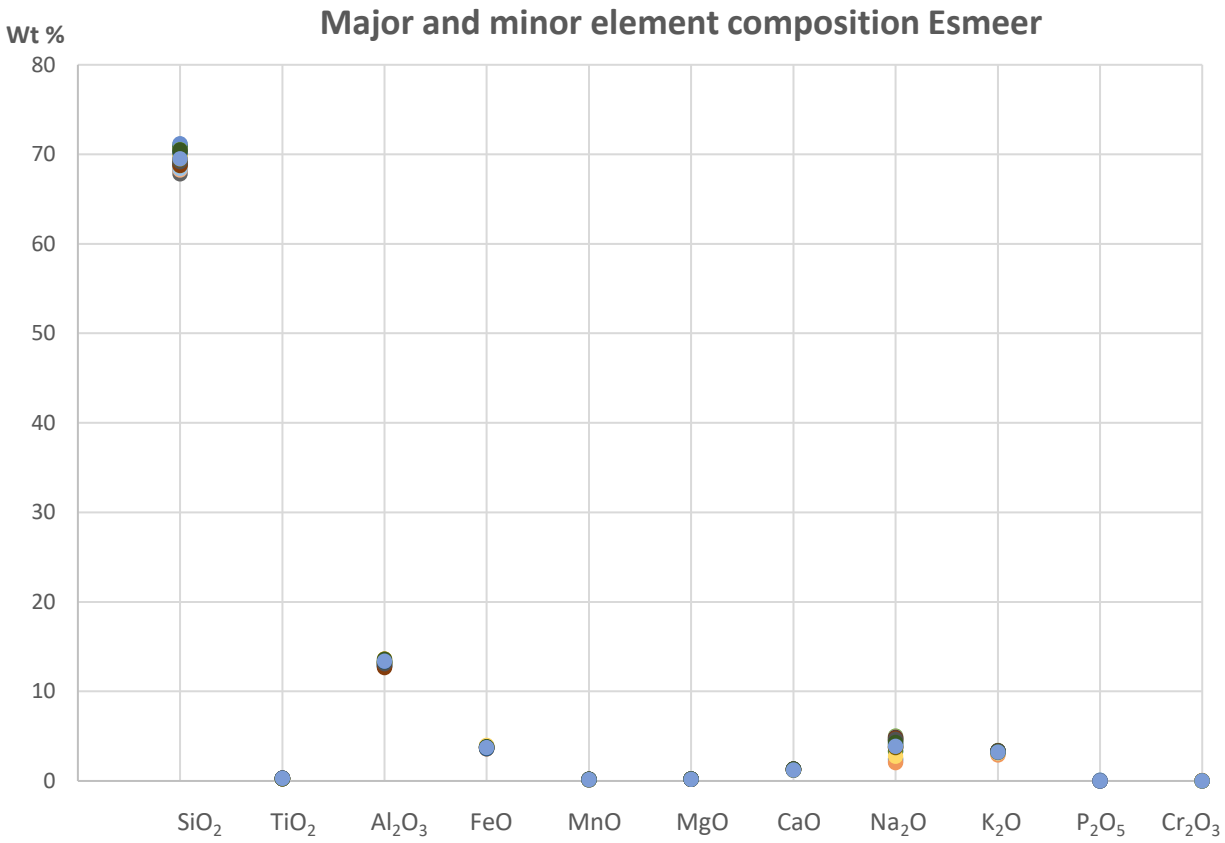

Fig. 11: *Major and minor element composition of encountered glass shards at 469-470 cm depth as established by WDS-EPMA, plotted as weight percentage per oxide. The six rejected measurements are excluded in this diagram.*

To correlate the encountered glass shards to known volcanic eruptions, the WDS-EPMA results are compared to major and minor element concentrations of previously researched tephra. The occurrence of 221 glass shards per cm^3 at this particular depth could point towards a correlation with the well researched Vedde Ash. Therefore the major and minor element concentration of Esmeer glass shards is compared to several tephra element concentrations correlated to the rhyolitic Vedde Ash. Six publications are used as data resource, which were all obtained using methods similar to this research (WDS-EPMA). These include two publications describing Vedde Ash in a location close to Esmeer (Hämelsee, Jones et al., 2018 & Kostverloren Veen, Davies et al., 2005).

Avarage weight percentages of each major or minor element measured by above mentioned publications are visible in table 7, including the total amount of measurements (n) and 1 sigma deviations (1σ). The wt% of P_2O_5 of shards at Kostverloren Veen and Soppensee are lacking in this table, because this element was not measured. Cr_2O_3 is not shown because this is only measured in this research and cannot be compared to other rhyolitic Vedde Ash measurements.

Source		SiO_2	TiO_2	Al_2O_3	FeO	MnO	MgO	CaO	Na_2O	K_2O	P_2O_5	TOTAL	n
Esmeer, NL	mean	69.91	0.26	13.00	3.67	0.15	0.19	1.25	4.05	3.22	0.00	95.57	32
This research	1σ	1.02	0.02	0.23	0.09	0.02	0.01	0.03	0.80	0.11	0.03	1.23	
Hämelsee, DE	mean	69.02	0.27	12.79	3.64	0.15	0.21	1.41	4.96	3.37	0.04	95.86	23
Jones et al. 2018	1σ	0.63	0.01	0.26	0.14	0.01	0.02	0.05	0.16	0.80	0.01	0.81	
Kostverloren Veen, NL	mean	70.19	0.27	13.10	3.75	0.15	0.21	1.29	4.63	3.40	-	97.01	15
Davies et al. 2005	1σ	0.68	0.04	0.13	0.09	0.02	0.02	0.07	0.17	0.07	-	0.88	
Rotmeer, DE	mean	69.81	0.27	13.29	3.73	0.13	0.20	1.30	5.11	3.43	0.04	97.31	35
Lane et al. 2012b	1σ	1.06	0.03	0.27	0.16	0.05	0.02	0.07	0.15	0.10	0.02	1.48	
Soppensee, CH	mean	70.66	0.28	13.55	3.66	0.15	0.21	1.28	4.65	3.44	-	97.89	5
Blockley et al. 2007	1σ	0.84	0.02	0.19	0.09	0.04	0.01	0.06	0.19	0.14	-	1.22	
Meerfelder Maar, DE	mean	72.14	0.30	13.59	3.81	0.17	0.21	1.36	4.94	3.45	0.04	97.31	7
Lane et al. 2015	1σ	0.26	0.03	0.16	0.13	0.03	0.01	0.07	0.35	0.04	0.02	1.72	
Crudale Meadow, UK	mean	71.11	0.28	13.08	3.71	0.15	0.19	1.29	5.00	3.47	0.02	98.31	21
Timms et al. 2018	1σ	0.84	0.01	0.26	0.19	0.01	0.03	0.08	0.17	0.09	0.01	0.95	

Table 7: *Summary of WDS-EPMA results (wt%) of Esmeer and five other locations that contained Vedde Ash. The list of elements is lacking Cr since this element is not measured by any of the five publications. All errors are shown as 1σ for consistency.*

As visualization of the element concentrations of table 7, a diagram is made in figure 12 showing the resemblance in element concentration of the glass shards of Esmeer and selected publications. A selection of biplots (figure 13) displays the spreading of WDS-EPMA measurements of Esmeer as well as measurements of four other sites containing rhyolitic Vedde Ash.

In general, as table 7 and figures 12 and 13 show, the majority of the major and minor element concentrations of the glass shards of Esmeer show great similarity to the element concentration of rhyolitic Vedde Ash as measured in the six mentioned publications. Na_2O forms an exception to this, with a mean wt% of only 4.05 compared to 4.63 - 5.11 wt% in previous research. Its 1σ value is significantly higher as well. Besides Na_2O, K_2O has a slightly lower wt% as well.

The possible reasons for sodium loss (and potassium loss to a lesser extent) are further discussed in chapter 6.1.

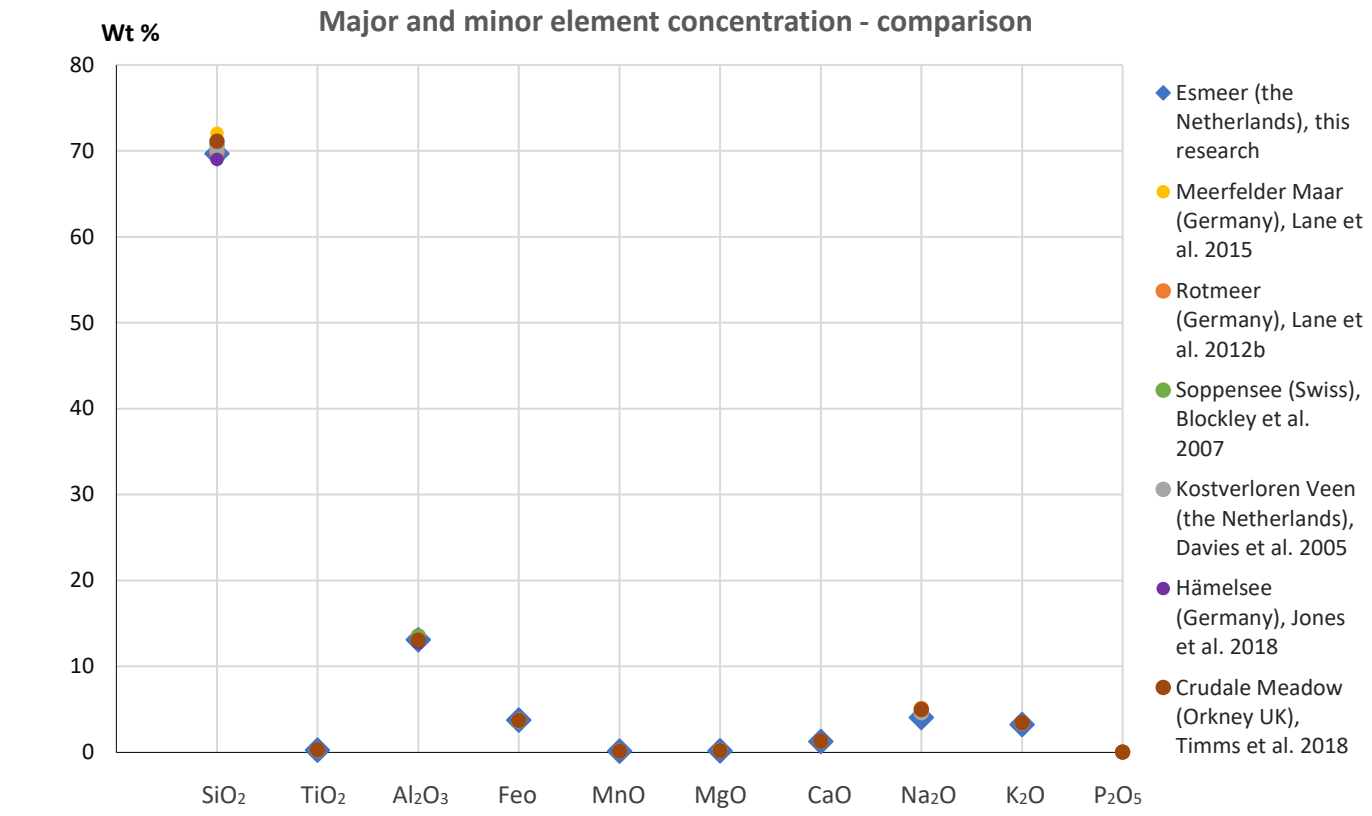

Fig. 12: *Comparison of major and minor element concentrations as measured by EPMA-WDS. Shards of lake Esmeer are compared to previously researched Vedde Ash. The data of table 7 is used as input.*

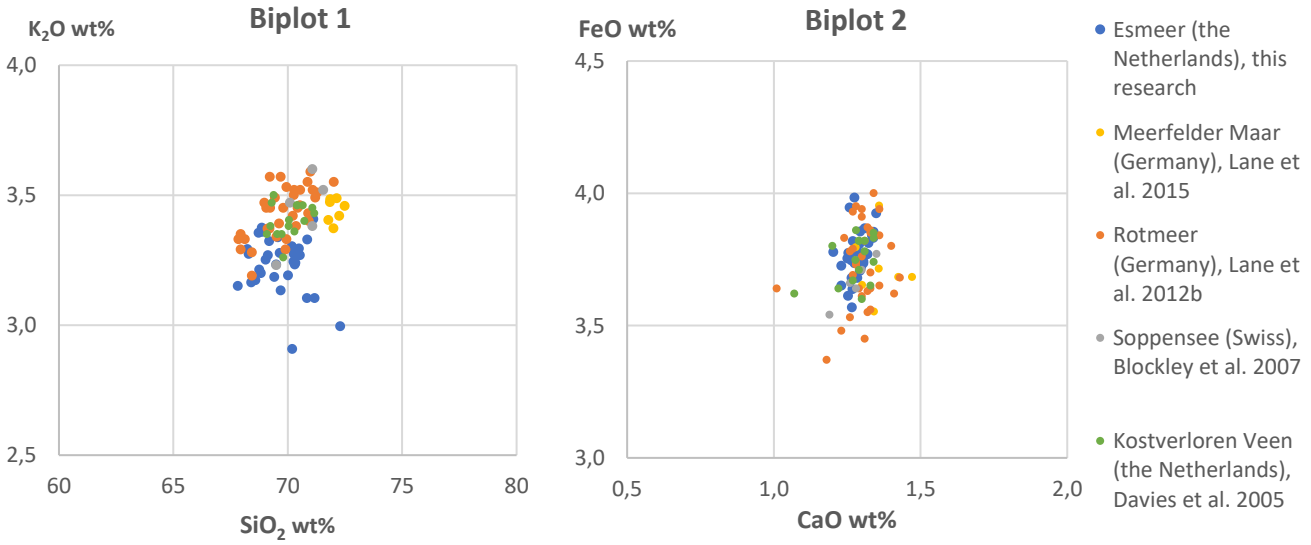

Fig. 13: *Biplots of wt% element concentrations of Esmeer, Meerfelder Maar (Lane et al., 2015), Rotmeer (Lane et al., 2012b), Soppensee (Blockley et al., 2007), and Kostverloren Veen (Davies et al., 2005).*

It should be noted that all Vedde Ash data from earlier publications used in table 7 and figures 12 and 13, are rhyolitic end members of the bimodular Vedde Ash. In comparison to the rhyolitic end member, the basaltic one is characterized by lower weight percentage of SiO_2 (47 wt%), Na_2O (3 wt%) and K_2O (0.7 wt%) and higher weight percentage of FeO (14 wt%), CaO (10 wt%), TiO (4.5 wt%) and MgO (5 wt%). This does not resemble the element concentration of the Esmeer glass shard, therefore the basaltic end member of Vedde Ash is disregarded for potential correlation.

5.3 Trace element concentration

In addition to the major and minor element concentration, the trace element concentration of the potentially Vedde Ash shards from Esmeer are measured by LA-ICP-MS. The results of these measurements are shown in table 8. The SE maps produced by EPMA were used as navigation during these measurements and contain an overview of which measurement is taken in which shard. The maps are included in appendix D.

In total, 25 measurements were performed on 16 different tephra shards so 9 shards were measured twice. Of these 25 measurements, three measurements are rejected: 1g, 1h, and 3c. The main reason for this data rejection are the large error estimates (indicated by 1σ, as calculated by GLITTER) that these measurements show for the individual trace element concentrations. A table of all 1σ values is available in appendix E. When looking into these 1σ values in detail, a certain trend is visible for each trace element. Some of the measurements show large 1σ values that significantly deviate from the general trend shown by a particular trace element. The Rb measurements are an example for this. The majority of the Rb measurements have 1σ values well between 4 and 9, while 1g and 1h show 1σ values of respectively 18 and 50. Ig and 1h show the most amount of 1σ deviations as well as the largest 1σ deviations. For 3c this was more moderate. For 1g and 1h, the yield of the measurement was probably too low. These measurements had the smallest spot size (10 µm versus 20 and 30 µm for the other measurements) due to the small shard sizes. Consequently, these measurements had the shortest selected range in GLITTER (3 and 4 seconds). This is not applicable to 3c, since it was measured with a spot size of 20 µm and had a stable range of an appropriate duration (20 seconds). This measurement could have suffered from impurities present on the shard. Besides these three measurements, 22 measurements were classified as reliable and useful for data analysis. It is also important to know that two other trace elements are measured by LA-ICP-MS which are not shown in table 8: V and Cr. The measurements of V and Cr are regarded as unreliable since the concentrations were often below the detection limit of the LA-ICP-MS. Their measured element concentrations are shown as well in appendix E, accompanied by their corresponding 1σ values.

	Rb	Sr	Y	Zr	Nb	Cs	Ba	La	Ce	Pr	Nd	Sm	Eu	Gd	Tb	Dy	Ho	Er	Tm	Yb	Lu	Hf	Ta	Pb	Th	U	spot size (µm)
1a	72	111	78	767	99	1	601	78	174	20	81	16	3	16	2	13	2	8	1	8	1	18	6	5	10	4	30
1c	80	113	67	667	88	1	688	88	172	21	68	16	4	17	2	13	3	9	1	7	1	22	8	7	12	3	30
1b	74	51	120	451	80	1	642	91	189	23	90	19	5	19	4	25	4	13	1	10	2	19	8	9	12	3	30
1d	82	126	91	938	116	1	653	92	198	25	91	17	3	16	3	17	3	9	2	7	1	22	7	7	12	3	30
1e	81	114	81	820	104	1	655	88	186	21	77	17	5	16	3	16	3	8	1	7	1	21	6	7	11	3	30
1f	96	124	74	762	104	2	693	89	167	21	73	25	4	20	2	15	4	5	3	2	1	13	6	8	10	3	30
2a	90	121	96	945	131	1	779	110	212	23	99	17	5	22	5	18	3	10	2	8	1	25	9	7	13	4	20
2b	85	128	91	849	98	1	609	95	208	23	90	15	2	8	2	18	5	7	1	8	1	15	5	6	14	4	20
3a	84	125	97	974	123	1	668	92	187	20	85	17	4	15	3	19	3	6	2	10	1	21	7	5	12	3	30
3d	91	129	85	896	110	1	653	90	193	24	81	22	5	15	3	18	4	9	2	7	1	26	7	6	12	3	20
3b	118	146	90	860	105	2	753	93	190	23	87	18	3	16	2	24	3	15	1	3	1	15	6	9	11	4	30
3e	77	126	95	915	113	1	625	89	190	23	85	15	4	19	2	14	4	8	2	11	1	20	7	5	12	3	30
3f	80	133	95	986	116	1	644	93	188	23	94	18	2	16	3	16	3	10	1	10	1	24	8	8	14	4	30
4a	86	121	88	839	102	1	658	96	199	24	85	17	3	15	3	11	3	9	2	9	1	19	6	8	12	4	30
4b	124	99	61	612	70	7	716	85	165	16	70	9	2	16	1	15	3	9	1	7	1	13	6	10	12	3	30
4c	86	104	70	731	98	1	625	86	179	18	73	12	2	16	3	19	4	8	2	7	1	19	6	7	11	3	20
4d	80	111	73	798	98	1	651	91	193	18	88	18	4	25	3	16	3	8	1	7	1	17	7	6	12	4	20
4e	79	134	117	1273	154	1	781	101	214	27	109	20	5	20	2	21	6	10	1	13	1	20	8	13	13	4	30
4f	70	109	93	1086	151	1	728	89	166	20	99	17	4	18	3	18	3	6	1	11	2	30	8	6	10	3	30
4g	81	99	70	788	113	1	807	101	176	18	70	18	4	20	3	21	4	8	1	7	2	28	9	10	14	3	30
4h	82	146	121	1375	167	1	691	95	224	29	142	25	4	16	3	20	4	12	2	17	2	29	9	10	13	4	30
4i	84	115	77	707	73	1	585	93	193	21	76	15	2	13	2	21	5	7	1	7	1	12	4	6	12	3	30
average	**85**	**118**	**88**	**865**	**110**	**1**	**678**	**92**	**189**	**22**	**87**	**17**	**4**	**17**	**3**	**18**	**4**	**9**	**1**	**8**	**1**	**20**	**7**	**7**	**12**	**3**	
rejected																											
1g	163	49	48	283	42	3	375	38	69	8	34	<5	8	<11	<2	16	<2	<3	<2	7	2	<2	4	5	5	10	10
1h	95	103	91	693	90	3	645	87	146	16	66	32	3	24	2	16	3	10	<3	29	<1	8	3	9	9	3	10
3c	106	124	81	1077	161	3	742	99	240	26	132	27	5	15	2	26	6	20	4	5	1	18	8	13	13	4	20

Table 8*: LA-ICP-MS results of the glass trace element concentration. The underscores in the mount column mark which measurements are performed on the same glass shard, since the majority of the shards is measured multiple times*

Trace elements are commonly present in Earth materials, hence the trace element concentration of Esmeer as measured by LA-ICP-MS does not yet tell anything about which trace elements are enriched. To compare this research' trace element concentration to primitive Earth material, the measured concentrations are normalised to trace element concentrations in the primitive mantle. The average trace elements concentrations presented in table 8 are normalised using values of the primitive mantle as established by Sun & McDonough (1989). The resulting graph is visible in figure 14, using a logarithmic scale for the normalised concentration. An overall enrichment of trace elements in the measured glass shards is apparent, varying between 5 and 180 times the primitive mantle values.

These measurements can be compared to other published trace element concentrations of Vedde Ash. Currently, only limited datasets on Vedde Ash trace element concentration are available. Lane et al. (2012b) presents the first single grain trace element analysis of both rhyolitic and basaltic Vedde Ash deposits in Kråkenes (Norway), Rotmeer (Germany) and Loch Ashik (Scotland), of which only Rotmeer contained mere rhyolitic Vedde Ash. Housley et al. (2011) published a small data set on trace element concentration of glass shards from Ahrenshöft (Germany). Since the deposition age of these shards is not established, no positive correlation

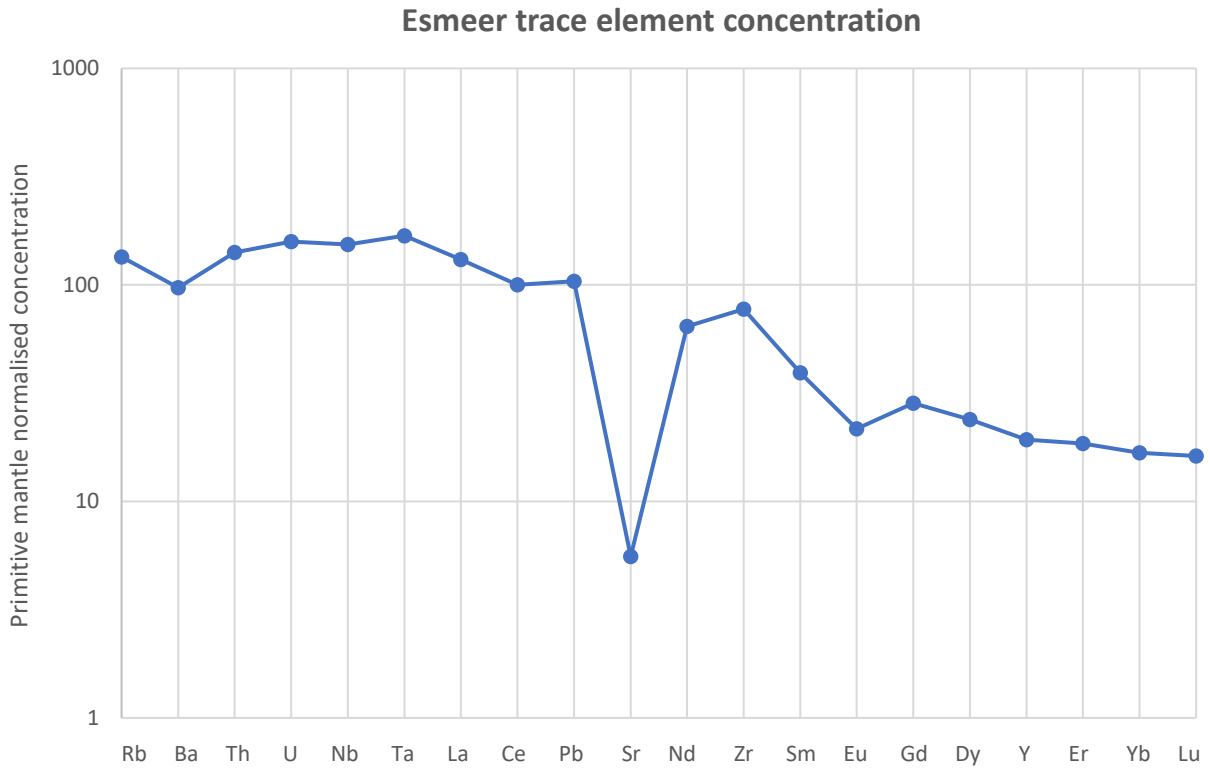

Fig. 14: *Primitive mantle normalised trace element concentration from lake Esmeer, based on average values as measured by LA-ICP-MS. Normalisation is based on the primitive mantle concentrations by Sun & McDonough (1989). Note the logarithmic scale on the y-axis.*

to Vedde Ash could be made. Nevertheless, the trace element concentrations are similar to the rhyolitic Vedde Ash of Lane et al. (2012b), so this dataset is taken into account as well for comparison to Esmeer data. A more recent publication by Lane et al. (2015) shows trace element concentrations for both rhyolitic and basaltic Vedde Ash in Meerfelder Maar (Germany).

Since the major and minor element compositions of the Esmeer glass shards correspond to the rhyolitic component of Vedde Ash, the Esmeer trace element data are compared to the rhyolitic trace element concentrations of previously mentioned literature in figure 15. As this diagram shows, the trace element concentrations of Rotmeer, Meerfelder Maar and Ahrenshöft resemble the Esmeer trace element concentration. Some deviations from the general trend is seen, Esmeer shows slightly higher average values of some trace elements (Pb, Dy, Y, Lu) and a lower average value for one element (Nb). However, these deviations are small and the Esmeer trace element concentrations seems to match with the previously established rhyolitic Vedde Ash trace element concentrations.

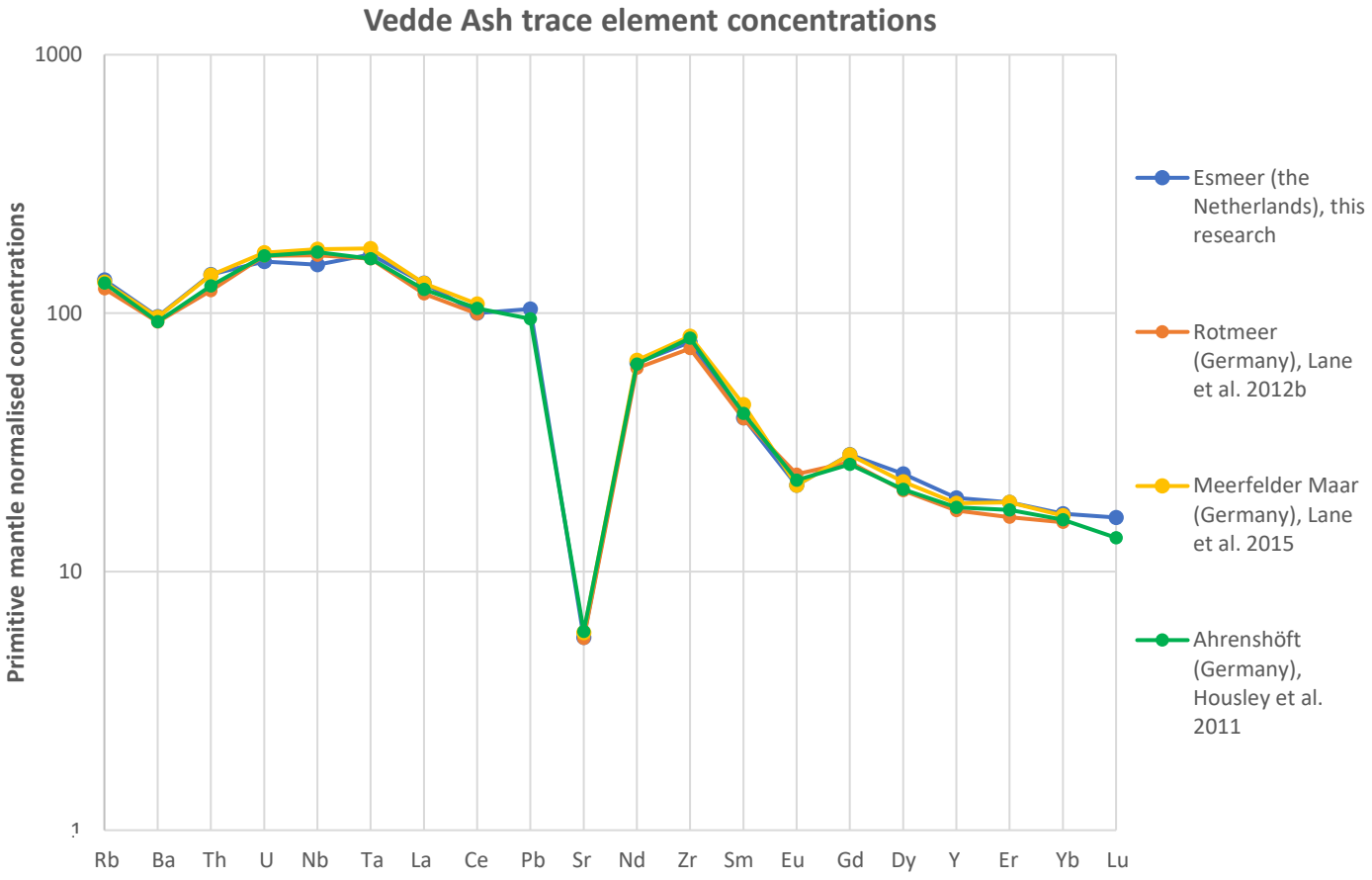

Fig. 15: *Trace element concentration of rhyolitic Vedde Ash in Rotmeer (Germany), Meerfelder Maar (Germany), and (potentially Vedde Ash) Ahrenshöft (Germany). Note the logarithmic scale of the y-axis. Values of the primitive mantle of Sun & McDonough (1989) are used to normalise all averaged trace element concentrations.*

The question rises whether the general trace element concentration in figure 15 is unique for Vedde Ash or whether it is a general trend for (Icelandic) rhyolitic tephra. To provide some insight in this, another trace element concentration diagram is plotted in figure 16. This diagram shows several trace element concentrations of Icelandic and rhyolitic tephra, of which the minor and major element concentrations are similar to Vedde Ash.

The diagram in figure 16 shows four distinct tephra layers. MD04 (specifically MD04-2822, 2385-2386 cm, Abbott et al., 2013) and LINK 16 (specifically LINK 16 735-737 cm, Abbott et al., 2014) originate from different source volcanos than Vedde Ash but have a major and minor element composition similar to Vedde Ash. However, as figure 16 shows, their trace element concentrations clearly deviates from the Esmeer trace element concentrations. This is different for the Dimna Ash, originally described by Koren et al. (2008) and further measured by Lane et al. (2015). This tephra layer is believed to originate from the Katla volcano (as is Vedde Ash) and shows a very similar trace element concentration trend as measured in the shards of lake Esmeer.

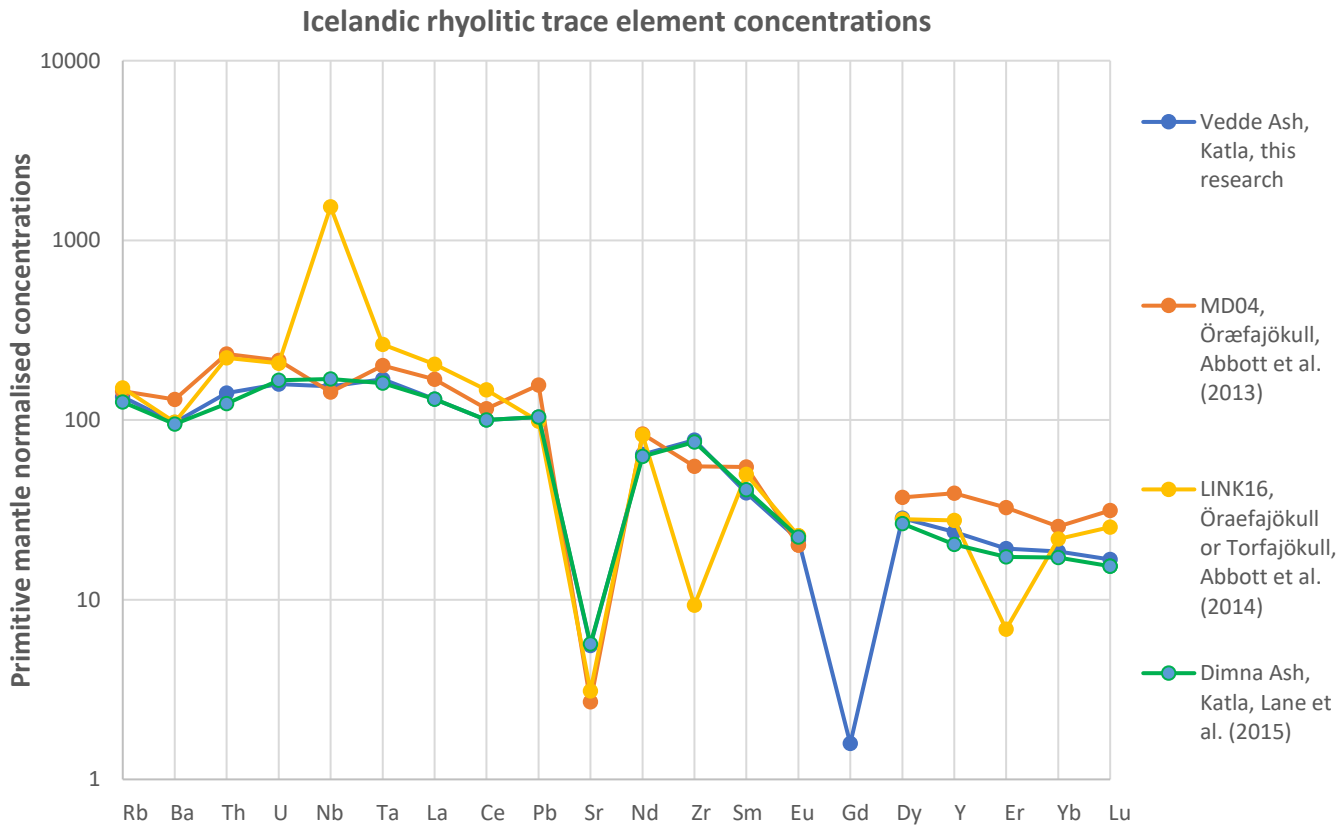

Fig. 16: *Trace element concentration of Icelandic rhyolitic tephra deposits. The legend indicates the name of tephra layer and its assumed source volcano.*

5.4 Vedde Ash and lithology

Figure 17 shows the LOI profile of Esmeer as measured prior to this study. The base of the sediment record (from 504 cm depth and upwards) shows a low organic content of circa 7 wt% until it rises to circa 50 wt% from 495 cm depth and upwards. Between 482 and 452 cm depth, the organic matter declines again to a low amount of circa 5 wt%. From 452 cm and upwards, the organic matter has risen again until about 90 wt%. The first increase in LOI is often correlated to the Bølling – Allerød interstadial and the second increase to the onset of the Holocene.

The depth containing the maximum concentration of the observed shards (469-470 cm) is indicated by a green line in figure 17. Since this maximum peak is also the basal peak of the tephra distribution, the green line represents the deposition timing of these shards in Esmeer as well.

As the figure shows, the shards occur in a part that only contains circa 5% organic matter. 95% of this part of the records is made up of sediments like sand and clay. According to the general trend often shown in these periods, the deposition of the measured shards probably occurred in the Younger Dryas.

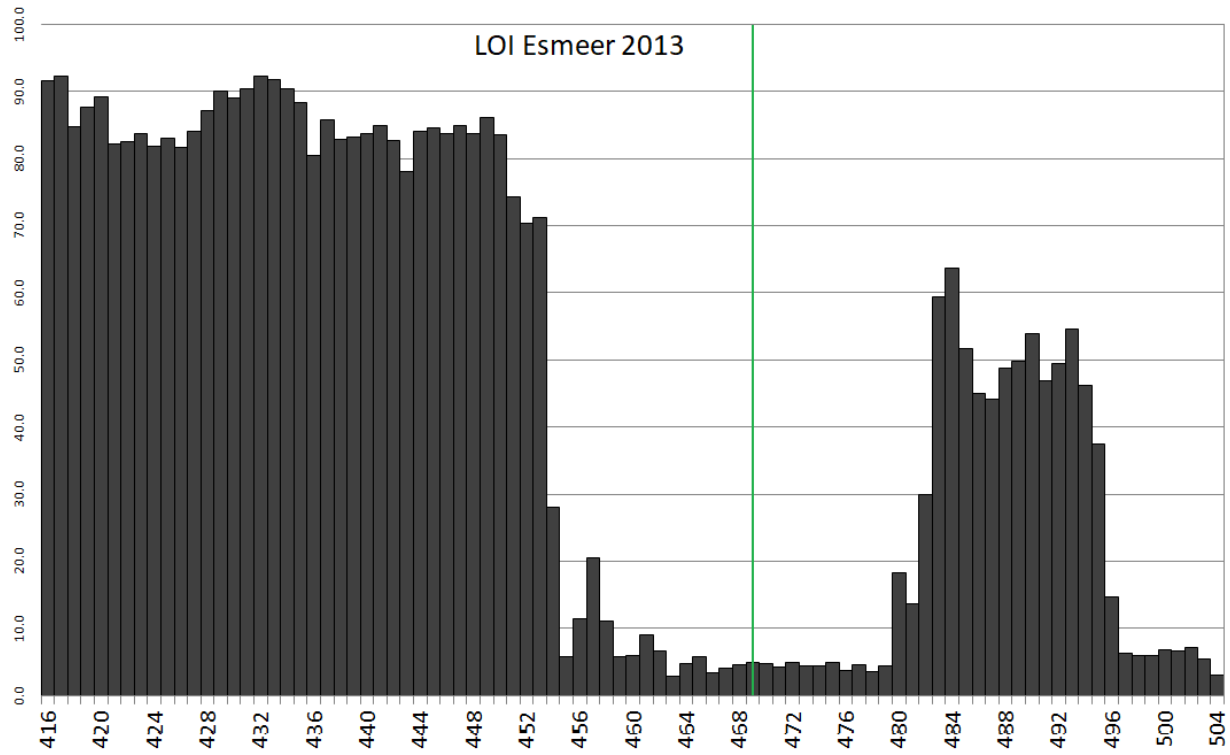

Fig. 17: *LOI (loss on ignition) diagram of Esmeer. The black boxes indicate what percentage of the original sample has vanished during the LOI process, representing the percentage of organic material present in the sample.*

For comparison, the LOI diagrams of two other locations containing Vedde Ash relatively close to Esmeer are depicted as well. Figure 18 shows an LOI profile of Hämelsee (Jones et al., 2018) and two of Kostverloren Veen (Davies et al., 2005), next to a smaller version of the LOI profile of Esmeer. The depth at which Vedde Ash was encountered in Hämelsee and Kostverloren Veen is marked by a green line. Vedde Ash is seen in the sandy part of the Hämelsee record, containing a relatively low amount of organic matter (LOI wt% of circa 15). This is different for the cores from Kostverloren Veen, where Vedde Ash is encountered at the transition from an organic part to a sandy part of the record (LOI wt% of circa 23 and 30). Although the LOI percentages of Esmeer and Hämelsee are different, they show similarities by the presence of glass shards (for Hämelsee yet confirmed as Vedde Ash) in the relatively low organic matter part of the sediment sequence.

5.5 Vedde Ash and palynology

A recently made palynological analysis of lake Esmeer (Zwier, master thesis, 2018) can give more details on the timing of and environment during the deposition of the measured glass shards. As shown in 4.7, several time periods are identified based on this pollen analysis. A small version of the Esmeer pollen diagram is shown in figure 19, which includes a green line marking the glass shard deposition. A detailed overview of the pollen analysis is included in appendix B. The basal peak of the glass shards at 469-470 cm represents the deposition timing, which falls within the range of the Younger Dryas, *Empetrum* phase (zone IIIb, 474 - 462.5 cm).

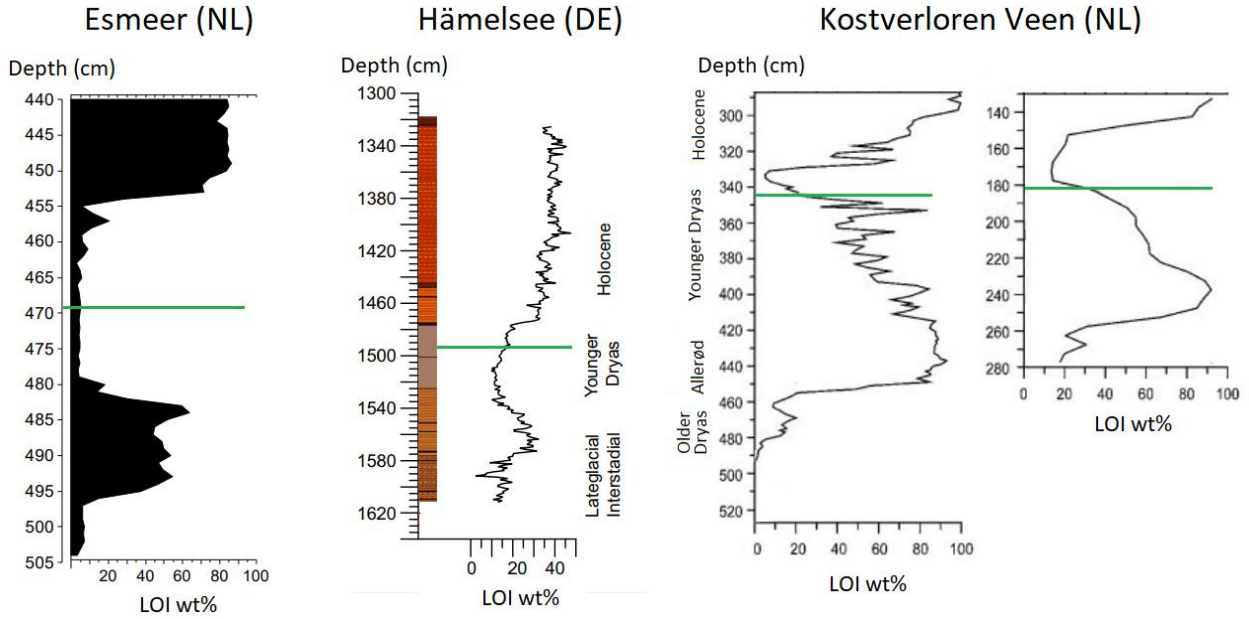

Fig. 18: *LOI (loss on ignition) diagrams of Esmeer, Hämelsee (Jones et al., 2018), and Kostverloren Veen (Davies et al., 2005). The green line indicates the depth at which Vedde Ash is encountered (and in the case of Esmeer, glass shards that are not yet confirmed as Vedde Ash).*

By this pollen diagram, the paleoenvironment at the time of shard deposition can be reconstructed. Around the time of shard (469-470 cm) deposition, pollen of trees (~75%), grasses (~10%), herbs (~7%), and heather (~8%) were present in Esmeer sediment record, and therefore in its close surroundings. The most abundant tree and shrub species around the lake where shard deposition occurred was birch (*Betula)*, accompanied by minorities of willow (*Salix*), pine (*Pinus*) and juniper (*Juniperus*). The herbs species were dominated by mugwort (*Artemisia)*, and to a lesser extent meadow-rue (*Thalictrum)*. Crowberry (*Empetrum*) was the main heather species. The vegetation is further characterized by the presence of riparian species such as sedges (Cyperaceae) ferns and mosses (monolete spores and *Polypodium vulgare*), and locally strongly rising values of green algae in the lake (Pediastrum).

Tephrochronological research can strengthen pollen analysis by adding time parallel markers to study paleoenvironmental fluctuations and by synchronizing pollen diagram of multiple locations. Before comparing the described paleoenvironment to other paleoenvironments at the timing of Vedde Ash deposits (as done by Lane et al., 2012a), it first needs to be discussed if the encountered glass shards are truly Vedde Ash shards.

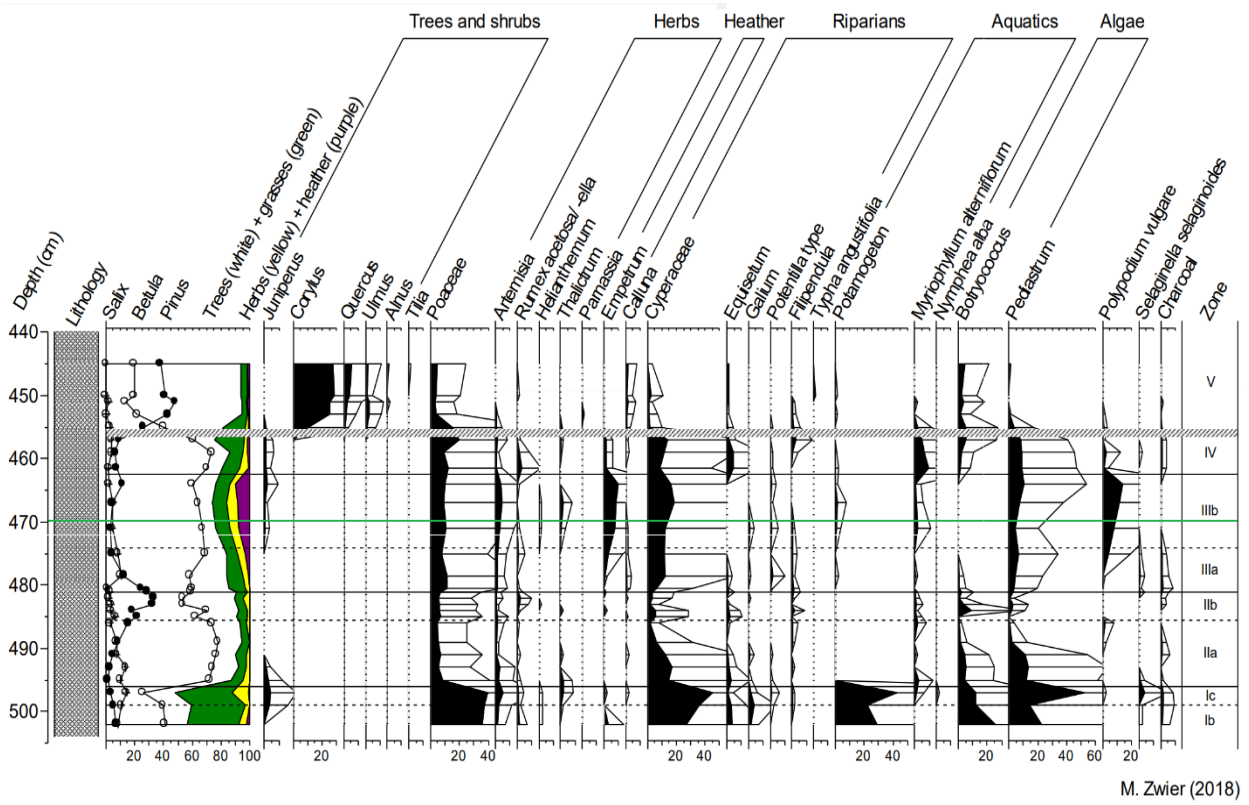

Fig. 19: *Section of pollen diagram of lake Esmeer after Zwier (master thesis, 2018). The depth of the basal shard peak is indicated by the green line.. Full pollen analysis available in appendix B.*

6. Discussion

Finding tephra layers in the Esmeer sediment record could provide new insights in the distribution and geochemical composition of these tephra layers and would strengthen the general position of tephrochronology. To conclude if the observed shards in this research are actually tephra shards, it is necessary to discuss whether the collected arguments for a tephra correlation are valid.

6.1 Vedde Ash measurements & correlation

This research has followed the general recommended protocol to conduct tephra related research as suggested by Turney et al. (2004) and Blockley et al. (2005). Sharply edged particles with a glassy appearance were encountered at a basal depth of 469-470 cm, with a maximum concentration of 221 shards per cm^3. Both the major and minor element concentration and trace element concentration of these shards show great similarities to the rhyolitic Vedde Ash as measured by aforementioned studies. The most deviating measurement is the element concentration of sodium (Na), which is only 4.05 wt% in this study instead of the range 4.63-5.11 wt% as measured by the studies used for comparison in this research (table 7). Its 1σ value (0.80) is considerably higher than all other 1σ values (0.15-0.35, table 7) of the mentioned previous studies. Figure 20 provides more details on the spreading of the Na_2O wt% values, showing all measurements from the lowest to the highest Na_2O wt%. This diagram shows that the majority of the measurements fall within the range of 3.7 to 5.0 wt%, and its average value is influenced by the six measurements below this range (varying between 2.0 – 3.4 Na_2O wt%).

A relatively low measured sodium concentration could indicate either an actual lower sodium concentration in the shards, a measurement flaw, or the occurrence of sodium loss before or during the EPMA measurements. The first option would weaken a potential correlation to Vedde Ash. Concerning the second option, no strong deviation was observed in the standard measurement (diopside). Since sodium is a volatile element, sodium loss is a reoccurring phenomenon in geochemistry. Therefore, the third option regarding sodium loss as a potential cause for a low sodium concentration should be taken into serious consideration. During EPMA measurements sodium loss can occur due to beam damage, causing depletion of alkalis and especially Na (e.g. Goodhew & Gulley, 1974).

The potential reasons for the occurrence of sodium loss in this research, might also be the cause for the slightly lower amount of K_2O (3.22 wt% in comparison to 3.37-3.47 wt% of previous research, table 7). An extra biplot is created (figure 21) that indicates a positive correlation between the wt% of Na_2O and K_2O. It is likely that a single process, either prior or during the

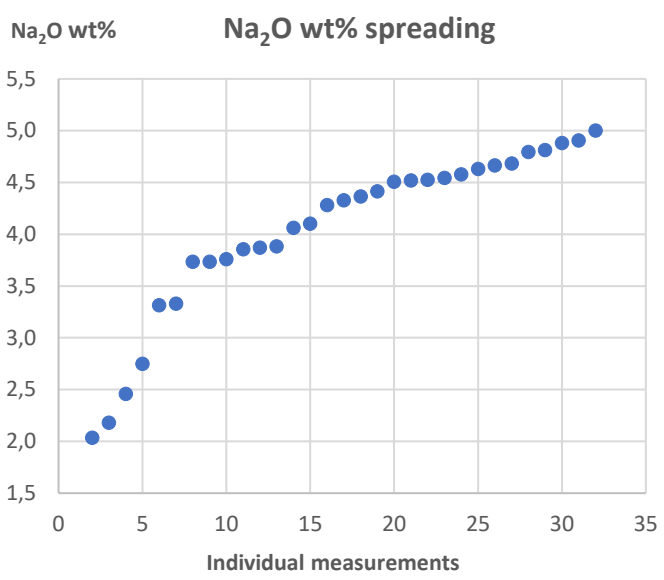

Fig. 20: *Na_2O wt% per individual WDS-EPMA measurement.*

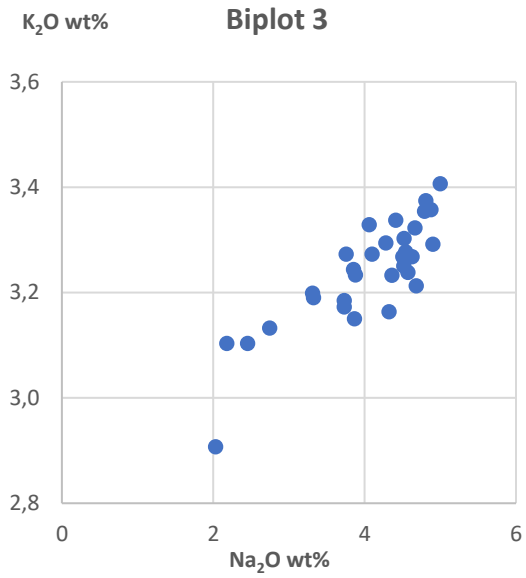

Fig. 21: *Biplot showing correlation between K_2O wt% and Na_2O wt% as measured by WDS-EPMA.*

measurements, caused both the sodium and potassium loss in the Esmeer glass shards, although potassium is less affected by this.

The potential reasons for the occurrence of sodium loss in this research, might also be the cause for the slightly lower amount of K_2O (3.22 wt% in comparison to 3.37-3.47 wt% of previous research, table 7). An extra biplot is created (figure 21) that indicates a positive correlation between the wt% of Na_2O and K_2O. It is likely that a single process, either prior or during the measurements, caused both the sodium and potassium loss in the Esmeer glass shards, although potassium is less affected by this.

To minimise sodium loss during this EPMA measurements, Na was included in the first batch of EPMA measurements (as explained in 4.5.3). Further minimisation of sodium loss during EPMA measurements is an interplay of its measurement settings. The EPMA spot size during this research varied between 3 to 5 µm, depending on the shard size. A smaller spot size reduces the yield and therefore the chance of including an impurity. However, this negatively affects Na measurements since Na loss can be reduced by a larger spot size. Table 9 contains an overview of the average Na_2O wt% per spot size. The average Na_2O wt% for all measurements performed with a 5 µm spot size is 4.29 wt% (1σ = 0.63), which is higher than the Na_2O wt% average of all measurements (4.05 wt%, 1σ = 0.80). The average Na_2O wt% of spot size 5 µm may be more reliable for Na_2O measurements and therefore more accurate than the average Na_2O wt% of all measurements. Still, this value is lower than the Na_2O wt% of previously researched Vedde Ash.

spot size (µm)	Na_2O wt%	1σ	n
3	3.66	0.33	5
4	2.11	0.10	2
5	4.29	0.63	24
3, 4 & 5	4.05	0.80	24

Table 9: *Average wt% and 1σ of Na_2O per spot size (varying from 3 to 5 µm)*

Options to minimise sodium loss in future research are increasing the spot size, or make reliable use of narrow beam diameters by using extremely low beam currents (Hayward, 2012).

Sodium (and potassium to a lesser extent) loss could also have occurred prior to the measurements due to degradation in its residence environment (e.g. Wolff-Boenisch et al., 2004). The shards of Esmeer resided in an acidic environment of clay, gyttja and sand, which can affect the glass shards by dissolution. In this case, only sodium and potassium are affected by this because all other element do not show any signs of loss or degradation.

Aside from the deviating sodium (and potassium to a lesser extent) concentration, the established element concentrations of the shards in the sediment record of Esmeer are in good agreement with those of rhyolitic Vedde Ash, and a positive correlation to this tephra layer is therefore possible. This data set would not be the first to be correlated to Vedde Ash despite of a low sodium concentration, since in Scotland tephra with a Na_2O wt% of 3,86 is found and correlated to rhyolitic Vedde Ash (Matthews et al., 2011). Unfortunately, this research did not include a mention nor a discussion regarding the sodium loss.

As previously explained, only establishing the geochemical composition of the encountered shards is not sufficient for a valid correlation to Vedde Ash. Previous studies indicate that several other tephra layers have major and minor element concentrations that are indistinguishable from the rhyolitic component of Vedde Ash. In that case, establishing the trace element concentration might be a useful tool to distinguish different tephra deposits. Diagram 16 compares the trace element concentration of Esmeer to other Icelandic and rhyolitic tephra deposits, of which the minor and major element concentration is similar to Vedde Ash. This diagram showed that the trace element concentration of Esmeer (likely originating from the Katla volcano) differs from the two presented trace element concentrations of tephra layers from other volcanic sources. The presented Dimna Ash is also believed to be originating from the Katla volcano and shows a trace element concentration similar to Esmeer. Therefore, the trace element concentration on itself might not be a decisive argument for a positive linkage to Vedde Ash, although it might be a very helpful tool in identifying different volcanic sources.

Tephra layers with similar minor and major element concentrations to Vedde Ash (and similar trace element concentrations when available) include the >15 ka BP Dimna Ash, the 11.2-11.8 ka BP tephra AF555 and the circa 8 ka BP Suðuroy tephra. Such chemically similar tephra layers can best be distinguished by deposition age. Both the LOI and palynology diagram indicate a deposition timing in the Younger Dryas (circa 12 900 to 11 700 yr BP). This would exclude both the >15 ka BP Dimna Ash and the 8 ka BP Suðuroy tephra. The AF555 tephra layer was encountered close to the top of the Younger Dryas, just prior to the onset of the Holocene (Matthews et al., 2011). However, looking at the positioning of the basal peak in the LOI diagrams of 5.5, the deposition timing of the encountered shards seems to be somewhere in the middle of the Younger Dryas. This is in agreement with the established age of Vedde Ash, 12.1 ka BP. Combining the results of the geochemical analysis and the deposition age as a result of the basal peak positioning in both the LOI and pollen diagrams, the glass shards encountered at depth 469-470 cm can be correlated with relatively high confidence to the rhyolitic component of Vedde Ash.

6.2 Implications of Vedde Ash correlation

A correlation of the shards at 469-470 cm depth to Vedde Ash adds a precise time marker to the Esmeer pollen diagram of Zwier (master thesis, 2018). This enables environmental reconstructions of Esmeer at the timing of tephra deposits and comparison to other locations. At the time of Vedde Ash deposit, pollen of trees (~75%), grasses (~10%), herbs (~7%), and heather (~8%) were present in the close surroundings of Esmeer. The most abundant tree species around Vedde Ash deposit was birch, accompanied by minorities of willow, pine and juniper. Due to the addition of Vedde Ash as a fixed point in time in this pollen diagram, this detailed environmental reconstruction can be compared to other time parallel paleoenvironments.

An example of synchronizing pollen analysis by tephrochronology is demonstrated by Lane et al. (2012a) who found both Vedde Ash and LST in sediment cores previously researched for pollen. As a result, both LST and Vedde Ash were drawn in pollen diagrams as time-parallel markers, visible in figure 17. By the time the Vedde Ash was deposited, Rotmeer, Soppensee, Rotsee, and Lago di Lavarone were dominated by pine woodlands, as indicated by their pine pollen of respectively circa 40, 45, 75, and 40%. Birch was less present at these sites, as indicated by the Betula pollen of respectively circa 10, 15, 15, and 10%. This was different for Lago Piccolo d'Avigliana, which was dominated by Betula (pollen circa 35%) and Pinus to a lesser extent (pollen circa 20%). This researched allowed to compare paleoenvironments north and south of the Alps and provided insights in reforestation trends, paleoclimate fluctuations, and atmospheric circulation. Similar comparisons can be made for Esmeer and its surroundings when other research sites close to Esmeer are researched for both pollen and tephra horizons as well, for example in Kostverloren Veen (Davies et al., 2005).

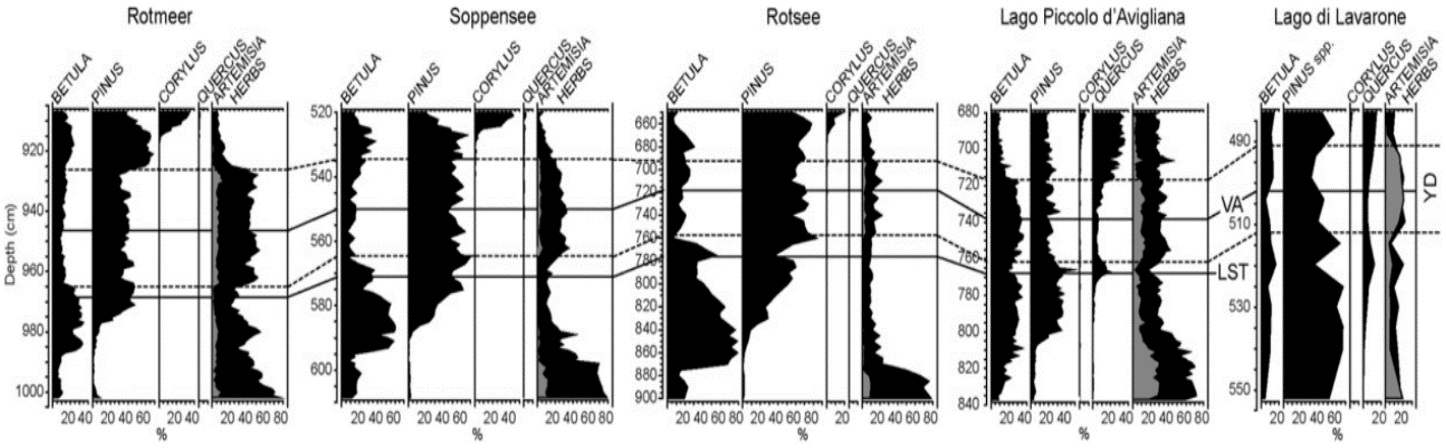

Fig. 22: *Pollen analysis including two tephra horizons: LST and Vedde Ash. After Lane et al., 2012a.*

The correlation to rhyolitic Vedde Ash also adds new geochemical data to tephra databases. The major and minor element concentration of rhyolitic Vedde Ash is already well established, but this research also provides a trace element concentration. The trace element concentration of the shards from Esmeer match well with those of previously researched Vedde Ash, only minor and probably neglectable deviations to the general trend are seen. Therefore, the results of this research strengthens the establishment of the Vedde Ash trace element concentration.

6.3 Laacher See Tephra measurements

Besides Vedde Ash, Laacher See Tephra was searched for as well in ranges 481-488 cm. No clear peak that significantly exceeds the human error was observed, although a slight increase in number of glassy shards was seen at depth 484-485 cm. Handpicking fresh shards at this depth was challenging for two reasons. The first is the appearance of the fresh shards, this is different from the shards that were treated by LOI that therefore appeared greenish. The surfaces of fresh shards contained more impurities and dirt and were less recognizable than the shards threatened by LOI. The second reason is the low shard concentration at this depth, which was significantly lower than for Vedde Ash depth (which therefore eases the handpicking process for Vedde Ash). The geochemical analyses did not yield trustworthy results, since the shards either could not be measured or showed a low total weight percentage. However, this does not necessarily mean that LST is not present in Dutch sediments. The deposition and intensity of tephra fall out is subject to processes like wind speed, wind direction and precipitation. After tephra fallout, the ecosystem affected by it will not act as a straightforward and passive archive. Ecosystems often form dynamic topographies, including an interplay of flora, fauna, and geomorphological processes. Therefore reworking of tephra deposits is possible on different scales, leading to an uneven distribution of tephra and discontinuous tephra layers. Significant differences in tephra concentration are hence encountered, even on a small scale (e.g. Watson et al., 2015; Davies et

al., 2005). Therefore, it might be possible that LST is present in the Netherlands, although the quantities may be low and therefore hard to detect. It should furthermore be noted that the Lateglacial-Early Holocene sediment record of Esmeer is only searched for target depths possibly containing Vedde Ash and LST. Other tephra horizons may be present in the non-researched part of the sediment record.

6.4 Future research

Several recommendations can be made for future research regarding tephrochronology.

Firstly, it is recommended to select EPMA measurements with great care to minimize the chance of sodium loss. For example, a lower beam current (nA) and a larger spot size of >5 µm when possible can be selected. If the same mounts are measured by both EPMA and LA-ICP-MS, this may cause overlap in the measured shard surfaces. This is discouraged by Pearce et al. (2014) since the surface of tephra shards may be damaged by EPMA beam radiation. However, since cryptotephra typically consist of small sized shards, this is nearly impossible to avoid.

Secondly, this research can be used as input for future research in time parallel paleo-environmental comparisons, since a detailed pollen diagram of Esmeer including the Vedde Ash deposit is now available. Further researching sediment cores for both the presence of pollen and tephra horizons is therefore required.

Thirdly, further researching trace element concentrations of tephra horizons is required. Icelandic rhyolitic tephra deposits with similar major and minor element concentrations might be distinguishable by their trace element concentrations. Further researching trace element concentrations of tephra deposits of different source volcanos, will provide insight in whether trace element concentrations have unique ranges per volcanic system. Further researching trace element concentrations of tephra deposits of the same volcanic system, might indicate how trace element concentrations evolve over time.

Fourthly, future research to tephra horizons in general will further strengthen the existence of tephra databases and the usefulness of tephrochronology. Although LST was not encountered in this research it may still be useful to look for LST in an extended area, even in the Netherlands since the concentration of LST shards may vary on a short distance.

7. Conclusions

The Lateglacial-Early Holocene sediment sequence of Esmeer is researched for the presence Vedde Ash and Laacher See Tephra. No sufficient evidence is found for the presence of an LST horizon in this sequence, although glass shards are observed at the LST target depths.

A cryptotephra is encountered in the sediment sequence of Esmeer with a basal peak at 469-470 cm depth and a maximum concentration of 221 shards per cm^3 (in the fraction 30-200 µm). The glass shards appeared colourless to pale greenish or pink due to LOI, and were sharply and either tetragonal or wing-like shaped. The major, minor and trace element composition are consistent with those previously published as the rhyolitic component of Vedde Ash, although sodium (and to a lesser extent potassium) loss occurred prior or during this research' measurements. As shown in this research, geochemical analysis alone is not sufficient for a positive correlation to Vedde Ash. However, due to the additional established deposition age of mid Younger Dryas as derived from both the LOI profile and pollen diagram, the encountered cryptotephra can be linked to the rhyolitic component of Vedde Ash with high confidence.

By the correlation to Vedde Ash, this research further establishes the geochemical composition of Vedde Ash. Especially this research' trace element concentration can be of added value, since this is less often researched for Vedde Ash compared to its minor and major element concentration.

The paleoenvironment round lake Esmeer at the time of Vedde Ash deposit is dominated by trees (mainly birch), accompanied by lower amounts of grasses, herbs, and heather, as derived from the pollen diagram by Zwier (master thesis, 2018). The addition of the Vedde Ash deposit to this pollen diagram allows time-parallel paleoenvironmental comparisons between different areas.

8. References

Abbott, P. M., Austin, W. E., Davies, S. M., Pearce, N. J., & Hibbert, F. D. (2013). Cryptotephrochronology of the Eemian and the last interglacial–glacial transition in the North East Atlantic. *Journal of Quaternary Science*, *28*(5), 501-514.

Abbott, P. M., Austin, W. E., Davies, S. M., Pearce, N. J. G., Rasmussen, T. L., Wastegård, S., & Brendryen, J. (2014). Re-evaluation and extension of the Marine Isotope Stage 5 tephrostratigraphy of the Faroe Islands region: The cryptotephra record. *Palaeogeography, Palaeoclimatology, Palaeoecology*, *409*, 153-168.

Allan, A. S., Baker, J. A., Carter, L., & Wysoczanksi, R. J. (2008). Reconstructing the Quaternary evolution of the world's most active silicic volcanic system: insights from an ~ 1.65 Ma deep ocean tephra record sourced from Taupo Volcanic Zone, New Zealand. *Quaternary Science Reviews*, *27*(25), 2341-2360.

Alley, R. B., Meese, D. A., Shuman, C. A., Gow, A. J., Taylor, K. C., Grootes, P. M., White, J.W.C., Ram, M., Waddington, E.D., Mayewski, P.A. & Zielinski, G. A. (1993). Abrupt increase in Greenland snow accumulation at the end of the Younger Dryas event. *Nature*, *362*(6420), 527.

Bogaard, P. van den., & Schmincke, H. U. (1985). Laacher See Tephra: A widespread isochronous late Quaternary tephra layer in central and northern Europe. *Geological Society of America Bulletin*, *96*(12), 1554-1571.

Blockley, S. P. E., Lane, C. S., Lotter, A. F., & Pollard, A. M. (2007). Evidence for the presence of the Vedde Ash in Central Europe. *Quaternary Science Reviews*, *26*(25-28), 3030-3036.

Blockley, S. P. E., Pyne-O'Donnell, S. D. F., Lowe, J. J., Matthews, I. P., Stone, A., Pollard, A. M.,Turney, C.S.M. & Molyneux, E. G. (2005). A new and less destructive laboratory procedure for the physical separation of distal glass tephra shards from sediments. *Quaternary Science Reviews*, *24*(16-17), 1952-1960.

Brauer, A., Endres, C., & Negendank, J. F. (1999). Lateglacial calendar year chronology based on annually laminated sediments from Lake Meerfelder Maar, Germany. *Quaternary International*, *61*(1), 17-25.

Davies, S.M., Hoek, W.Z., Bohncke, S. J., Lowe, J., O'Donnell, S. P., & Turney, C. S. (2005). Detection of Lateglacial distal tephra layers in the Netherlands. *Boreas*, *34*(2), 123-135.

Davies, S.M., Turney, C.S.M., & Lowe, J.J., (2001). Identification and significance of a visible, basalt-rich Vedde Ash layer in a Late-glacial sequence on the Isle of Skye, Inner Hebrides, Scotland. Journal of Quaternary Science 16, 99e104.

Flemal, R. C. (1976). Pingos and Pingo Scars: Their Characteristics, Distribution, and Utility in Reconstructing Former Permafrost Environments. Quaternary Research, 53, 37–53.

Goodhew, P.J. & Gulley, J.E.C. (1974). The determination of alkali metals in glasses by electron probe microanalysis. *Glass Technology 15*: 123–126

Harms, E., & Schmincke, H. U. (2000). Volatile composition of the phonolitic Laacher See magma (12,900 yr BP): implications for syn-eruptive degassing of S, F, Cl and H2O. *Contributions to Mineralogy and Petrology*, *138*(1), 84-98.

Hayward, C. (2012). High spatial resolution electron probe microanalysis of tephras and melt inclusions without beam-induced chemical modification. *The Holocene*, *22*(1), 119-125.

Heiri, O., Lotter, A. F., & Lemcke, G. (2001). Loss on ignition as a method for estimating organic and carbonate content in sediments: reproducibility and comparability of results. *Journal of paleolimnology*, *25*(1), 101-110.

Holmes, G. W., Foster, H. L., & Hopkins, D. M. (1966). Distribution and age of pingos of interior Alaska. *Proceedings of International Conference on Permafrost, Lafayette, Indiana, 1963.* NAS-NRC Publication No. 1287, 88-93.

Housley, R. A., Lane, C. S., Cullen, V. L., Weber, M. J., Riede, F., Gamble, C. S., & Brock, F. (2012). Icelandic volcanic ash from the Late-glacial open-air archaeological site of Ahrenshöft LA 58 D, North Germany. *Journal of Archaeological Science*, *39*(3), 708-716.

Jones, G., Lane, C. S., Brauer, A., Davies, S. M., Bruijn, R., Engels, S., Halius, A., Hoek, W.Z., Merkt, J., Sachse, D., Turner, F., & Wagner-Cremer, F. (2018). The Lateglacial to early Holocene tephrochronological record from Lake Hämelsee, Germany: a key site within the European tephra framework. *Boreas*, *47*(1), 28-40.

Koren, J. H., Svendsen, J. I., Mangerud, J., & Furnes, H. (2008). The Dimna Ash—a 12.8 14C ka-old volcanic ash in Western Norway. *Quaternary Science Reviews*, *27*(1-2), 85-94.

Lane, C. S., Blockley, S. P. E., Lotter, A. F., Finsinger, W., Filippi, M. L., & Matthews, I. P. (2012a). A regional tephrostratigraphic framework for central and southern European climate archives during the Last Glacial to Interglacial transition: comparisons north and south of the Alps. *Quaternary Science Reviews*, *36*, 50-58.

Lane, C. S., Blockley, S. P., Mangerud, J. A. N., Smith, V. C., Lohne, Ø. S., Tomlinson, E. L., Matthews, I.P. & Lotter, A. F. (2012b). Was the 12.1 ka Icelandic Vedde Ash one of a kind?. *Quaternary Science Reviews*, *33*, 87-99.

Lane, C. S., Brauer, A., Martín-Puertas, C., Blockley, S. P., Smith, V. C., & Tomlinson, E. L. (2015). The Late Quaternary tephrostratigraphy of annually laminated sediments from Meerfelder Maar, Germany. *Quaternary Science Reviews*, *122*, 192-206.

Larsson, S. A., & Wastegård, S. (2018). The Laacher See Tephra discovered in southernmost Sweden. *Journal of Quaternary Science*, *33*(5), 477-481.

Lotter, A. F., & Birks, H. J. B. (1993). The impact of the Laacher See Tephra on terrestrial and aquatic ecosystems in the Black Forest, southern Germany. *Journal of Quaternary Science*, *8*(3), 263-276.

Lowe, D. J., & Hunt, J. B. (2001). A summary of terminology used in tephra-related studies.

Lowe, J. J., Rasmussen, S. O., Björck, S., Hoek, W. Z., Steffensen, J. P., Walker, M. J. C., Yu, Z. C., & Intimate Group. (2008). Synchronisation of palaeoenvironmental events in the North Atlantic region during the Last Termination: a revised protocol recommended by the INTIMATE group. *Quaternary Science Reviews*, *27*(1-2), 6-17.

Lowe, J. J., & Walker, M. J. (2000). Radiocarbon Dating the Last Glacial-Interglacial Transition (Ca. 14–9 14 C Ka Bp) in Terrestrial and Marine Records: The Need for New Quality Assurance Protocols 1. *Radiocarbon*, *42*(1), 53-68.

Mangerud, J., Furnes, H., & Jóhansen, J. (1986). A 9000-year-old ash bed on the Faroe Islands. *Quaternary Research*, *26*(2), 262-265.

Mangerud, J., Lie, S. E., Furnes, H., Kristiansen, I. L., & Lømo, L. (1984). A Younger Dryas ash bed in western Norway, and its possible correlations with tephra in cores from the Norwegian Sea and the North Atlantic. *Quaternary Research*, *21*(1), 85-104.

Matthews, I.P., Birks, H.H., Bourne, A.J., Brooks, S.J., Lowe, J.J., Macleod, A., & PyneO'Donnell, S.D.F., (2011). New age estimates and climatostratigraphic correlations for the Borrobol and Penifiler Tephras: evidence from Abernethy Forest, Scotland. Journal of Quaternary Science 26, 247e252.

Morgan, G. B., & London, D. (1996). Optimizing the electron microprobe analysis of hydrous alkali aluminosilicate glasses. *American Mineralogist*, *81*(9-10), 1176-1185.

Mortensen, A. K., Bigler, M., Grönvold, K., Steffensen, J. P., & Johnsen, S. J. (2005). Volcanic ash layers from the Last Glacial Termination in the NGRIP ice core. *Journal of Quaternary Science: Published for the Quaternary Research Association*, *20*(3), 209-219.

Newton, A. (1996). Tephrabase. A tephrochronological database. *Quaternary Newsletter*, 8-13.

Newton, A.J., Dugmore, A.J., & Gittings, B.M., (2007). Tephrabase: tephrochronology and the development of a centralised European database. Journal of Quaternary Science 22 (7), 737e743.

Pearce, N. J. (2014). Towards a protocol for the trace element analysis of glass from rhyolitic shards in tephra deposits by laser ablation ICP-MS. *Journal of Quaternary Science*, *29*(7), 627-640.

Ramsey, C. B., Albert, P. G., Blockley, S. P., Hardiman, M., Housley, R. A., Lane, C. S., Lee, S., Matthews, I.P., Smith, V.C., & Lowe, J. J. (2015). Improved age estimates for key Late Quaternary European tephra horizons in the RESET lattice. *Quaternary Science Reviews*, *118*, 18-32.

Schmincke, H. U., Park, C., & Harms, E. (1999). Evolution and environmental impacts of the eruption of Laacher See Volcano (Germany) 12,900 a BP. *Quaternary International*, *61*(1), 61-72.

Smith, D. G. W., & Westgate, J. A. (1968). Electron probe technique for characterising pyroclastic deposits. *Earth and Planetary Science Letters*, *5*, 313-319.

Sun, S. S., & McDonough, W. S. (1989). Chemical and isotopic systematics of oceanic basalts: implications for mantle composition and processes. *Geological Society, London, Special Publications*, *42*(1), 313-345.

Timms, R. G., Matthews, I. P., Palmer, A. P., & Candy, I. (2018). Toward a tephrostratigraphic framework for the British Isles: A Last Glacial to Interglacial Transition (LGIT c. 16-8 ka) case study from Crudale Meadow, Orkney. *Quaternary Geochronology*, *46*, 28-44.

Tomlinson, E. L., Thordarson, T., Müller, W., Thirlwall, M., & Menzies, M. A. (2010). Microanalysis of tephra by LA-ICP-MS—strategies, advantages and limitations assessed using the Thorsmörk Ignimbrite (Southern Iceland). *Chemical Geology*, *279*(3), 73-89.

Turney, C. S., Harkness, D. D., & Lowe, J. J. (1997). The use of microtephra horizons to correlate Late-glacial lake sediment successions in Scotland. *Journal of Quaternary Science: Published for the Quaternary Research Association*, *12*(6), 525-531.

Turney, C. S., Lowe, J. J., Davies, S. M., Hall, V., Lowe, D. J., Wastegård, S., Hoek, W.Z. & Alloway, B. (2004). Tephrochronology of Last Termination sequences in Europe: a protocol for improved analytical precision and robust correlation procedures (a joint SCOTAV–INTIMATE proposal). *Journal of Quaternary Science*, *19*(2), 111-120.

Vorren, K. D., Elverland, E., Blaauw, M., Ravna, E. K., & Jensen, C. A. (2009). Vegetation and climate c. 12 300–9000 cal. yr BP at Andøya, NW Norway. *Boreas*, *38*(3), 401-420.

Waagstein, R., & Jóhansen, J. (1968). Tre vulkanske askelag fra Færøerne. *Age*, *100*, 14.

Walker, M. (2016). INTIMATE (Integration of Ice-core, Marine and Terrestrial Records) 20 Years on: Retrospect and Prospect. *Scottish Geographical Journal*, *132*(2), 164-170.

Wastegård, S, (2002). Early to middle Holocene silicic tephra horizons from the Katla volcanic system, Iceland: new results from the Faroe Islands. Journal of Quaternary Science 17, 723e730

Wastegård, S., Wohlfarth, B., Subetto, D. A., & Sapelko, T. V. (2000). Extending the known distribution of the Younger Dryas Vedde Ash into northwestern Russia. *Journal of Quaternary Science: Published for the Quaternary Research Association*, *15*(6), 581-586.

Watson, E. J., Swindles, G. T., Lawson, I. T., & Savov, I. P. (2015). Spatial variability of tephra and carbon accumulation in a Holocene peatland. *Quaternary Science Reviews*, *124*, 248-264.

Wolff-Boenisch, D., Gislason, S. R., Oelkers, E. H., & Putnis, C. V. (2004). The dissolution rates of natural glasses as a function of their composition at pH 4 and 10.6, and temperatures from 25 to 74 C. *Geochimica et Cosmochimica Acta*, *68*(23), 4843-4858.

Zwier, M. (2018). Substrate control on the Lateglacial and Early Holocene lithological and palynological fill of multiple pingo remnants in the Netherlands (*master's thesis*). Retrieved from: https://dspace.library.uu.nl/handle/1874/368064

Appendix A

Additional information figure 3 in section 2.3 (after Lane et al., 2012b).

This map shows locations where Vedde Ash, Suðuroy tephra, Dimna Ash and AF555 tephra have been identified in stratified terrestrial sites. Sites of samples used in Lane et al. (2012b) are marked with *. Grey shaded area demarks the extent of fallout deposits of Vedde Ash as known in 2012. The black outlined box highlights the areas of western Norway that contain Vedde Ash as a visible layer.

Numbered sites as followings:

1. NGRIP
2. Lake Torfadalsvatn
3. Kråkenes
4. Dimnamyra
5. Karelian Isthmus
6. Lake Madtjärn
7. Lake Götejön
8. Fågelmossen
9. Högstorpsmossen
10. Lake Kullatorpssjön
11. Loch an t'Suidhe
12. Druim Loch
13. Loch Ashik
14. Lochan An Druim
15. Borrobol
16. Abernethy Forest
17. Tynaspirit West
18. Whitrig Bog
19. Roddans Port
20. Kostverloren Veen
21. Endinger Bruch
22. Marais de la Maxe
23. Lac de Sewen
24. Rotmeer
25. Soppensee
26. Rotsee
27. Lago Piccolo di Avigliana
28. Lavarone
29. Lake Bled
30. Hovsdalur
31. Vestvågøy
32. Lake Æråsvatn

A number of marine core locations where Vedde Ash (or North Atlantic Ash Zone 1) has been reported are also shown.

Appendix B

Full pollen diagram Esmeer (after Zwier, 2018). The basal peak of the glass shards at 469-470 cm (correlated to rhyolitic Vedde Ash) is indicated by the green line.

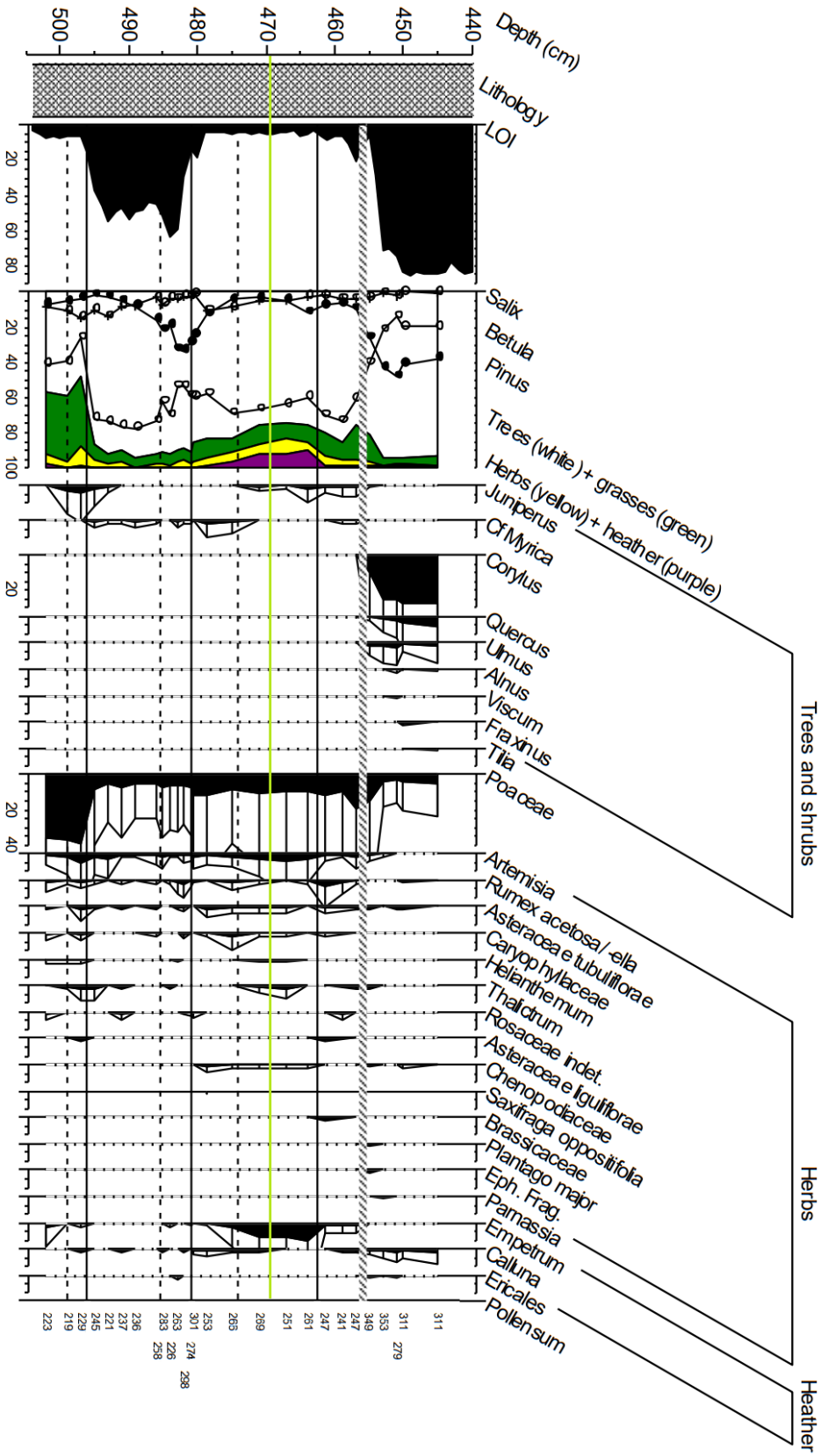

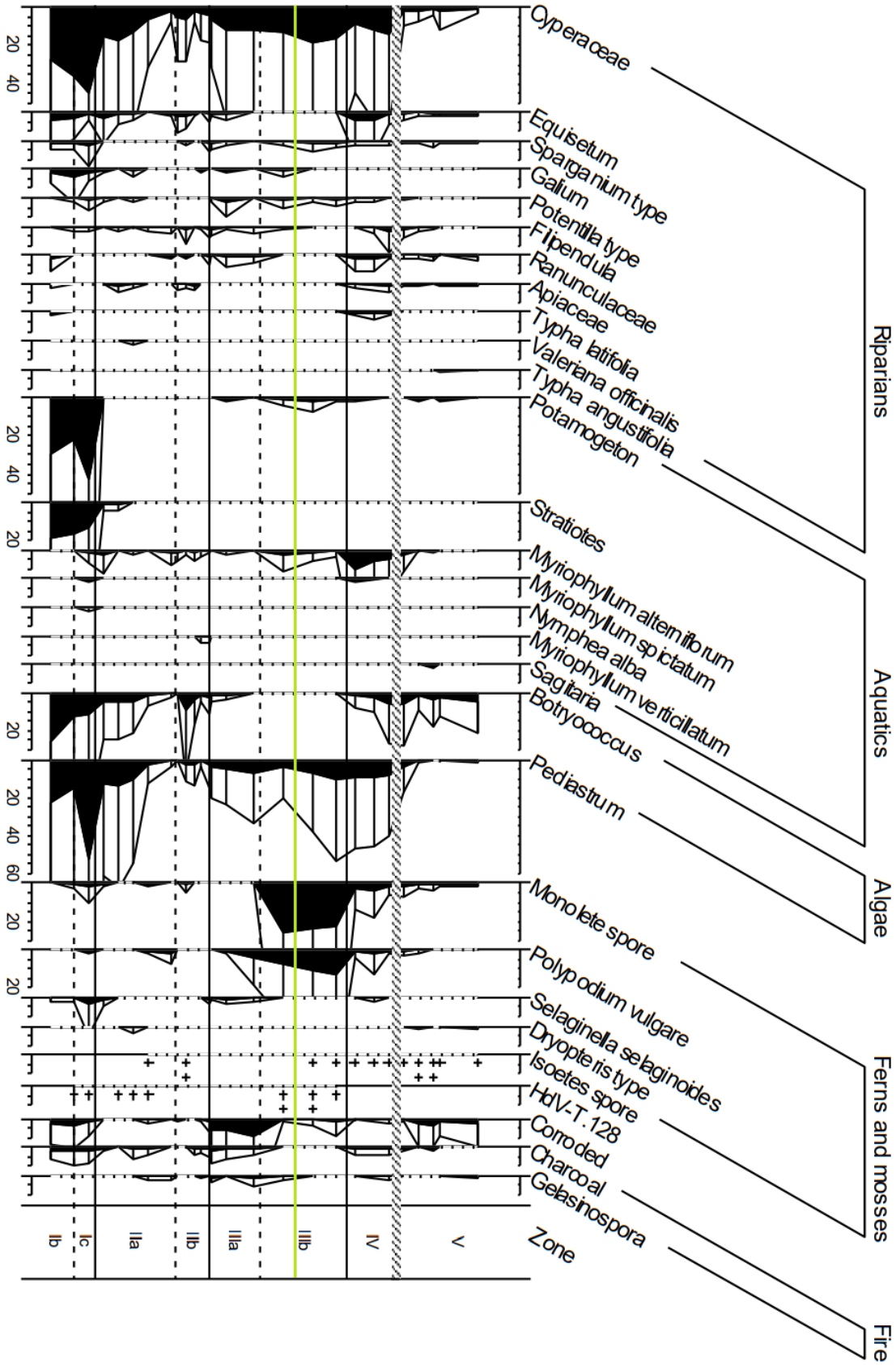
Cyperaceae
Equisetum
Sparganium type
Galium
Potentilla type
Filipendula
Ranunculaceae
Apiaceae
Typha latifolia
Valeriana officinalis
Typha angustifolia
Potamogeton
Stratiotes
Myriophyllum alterniflorum
Myriophyllum spictatum
Nymphea alba
Myriophyllum verticillatum
Sagitaria
Botryococcus
Pediastrum
Monolete spore
Polypodium vulgare
Selaginella selaginoides
Dryopteris type
Isoetes spore
HdV-T.128
Corroded
Charcoal
Gelasinospora
Zone
Riparians
Aquatics
Algae
Ferns and mosses
Fire
20
40
60
Ib
Ic
IIa
IIb
IIIa
IIIb
IV
V

Appendix C

Table of % Error per element as measured by WDS-EPMA.

	Si	Ti	Al	Fe	Mn	Mg	Ca	Na	K	P	Cr
1.6	0.28	6.89	0.65	1.60	17.34	8.40	1.39	1.17	0.77	-739.46	-155.36
1.7	0.28	7.06	0.65	1.61	11.76	6.67	1.39	1.72	0.81	-206.57	-132.56
1.8	0.28	6.58	0.65	1.68	13.88	7.12	1.43	1.36	0.80	108.83	1374.29
1.9	0.28	6.94	0.66	1.62	16.11	6.78	1.45	1.34	0.80	-1145.40	105.82
2.1	0.27	6.65	0.65	1.58	13.97	6.90	1.38	2.39	0.82	-268.61	-82.74
2.2	0.28	7.08	0.66	1.60	15.81	6.85	1.41	1.36	0.79	-212.95	95.28
2.3	0.28	6.50	0.65	1.63	14.02	7.09	1.47	1.31	0.78	1232.51	-94.11
2.4	0.28	6.49	0.65	1.60	11.65	7.34	1.40	1.83	0.81	308.23	-45.81
2.5	0.28	6.51	0.65	1.61	12.78	7.42	1.42	1.89	0.84	609.66	2486.10
3.1	0.28	7.52	0.65	1.58	14.89	6.49	1.44	1.26	0.79	190.97	163.69
3.2	0.28	7.22	0.65	1.62	13.86	7.29	1.43	1.23	0.79	-84.39	217.23
3.3	0.28	7.12	0.65	1.64	14.11	7.44	1.44	1.24	0.78	308.50	-410.65
3.4	0.28	6.73	0.64	1.61	19.30	6.81	1.43	1.22	0.79	159.47	98.88
3.5	0.28	7.53	0.66	1.63	12.78	7.05	1.41	1.24	0.79	155.13	-87.80
3.6	0.28	6.77	0.65	1.61	14.66	6.44	1.40	1.23	0.78	-74.10	54.27
3.7	0.28	7.35	0.65	1.63	17.03	6.57	1.42	1.23	0.79	-419.65	-102.59
3.8	0.28	6.63	0.64	1.62	14.97	7.11	1.43	1.35	0.79	68.02	-48.08
3.9	0.28	7.09	0.66	1.64	13.00	6.99	1.42	1.45	0.80	37.03	-76.50
3.1	0.28	6.22	0.65	1.65	15.62	7.13	1.44	1.46	0.80	-221.70	79.61
4.1	0.28	7.10	0.66	1.61	10.94	7.64	1.42	1.20	0.77	99.84	-163.54
4.2	0.28	6.75	0.66	1.62	15.02	7.22	1.40	1.19	0.78	-324.96	-43.42
4.3	0.28	6.58	0.66	1.64	16.11	6.60	1.43	1.25	0.78	321.17	155.90
4.4	0.28	7.42	0.65	1.58	11.56	7.70	1.43	1.61	0.80	-97.44	-79.79
4.5	0.28	7.41	0.66	1.66	14.43	7.71	1.42	1.26	0.80	396.00	-33.43
4.6	0.28	7.51	0.65	1.62	14.97	7.15	1.45	1.21	0.79	-91.47	-58.64
4.7	0.28	6.25	0.66	1.62	11.48	7.46	1.40	1.19	0.78	545.92	-138.31
4.8	0.28	7.24	0.66	1.62	14.24	7.88	1.41	1.20	0.78	-278.67	-82.47
4.9	0.28	5.94	0.65	1.64	11.79	6.79	1.42	1.22	0.78	189.07	-79.20
4.10	0.28	6.91	0.64	1.65	13.90	7.08	1.46	1.36	0.80	-6823.30	-39.93
4.11	0.28	6.73	0.65	1.65	13.78	7.77	1.44	1.30	0.79	-41.68	-149.35
4.12	0.28	6.77	0.64	1.60	12.11	6.96	1.39	1.27	0.78	-50.57	92.16
4.13	0.28	6.43	0.65	1.63	14.51	7.65	1.46	1.34	0.79	177.48	3883.33
rejected data											
1.1	0.29	6.89	0.69	1.66	13.09	6.84	1.46	1.35	0.83	-176.87	-100.51
1.2	0.31	7.42	0.76	1.75	12.68	8.43	1.55	1.55	0.86	197.81	109.34
1.3	0.31	7.03	0.75	1.76	24.69	9.37	1.59	1.89	0.88	100.19	-142.44
1.4	0.27	14.88	0.70	2.28	31.54	-269.54	2.17	1.42	0.83	-34.74	-161.36
1.5	0.27	12.73	0.70	2.24	26.90	96.60	2.11	1.44	0.82	-47.23	1319.65

Appendix D

Secondary Electron (SE) maps of mounts 1, 2, 3, and 4 (Vedde Ash target depths). Images are created by EPMA-SE. Each map shows the location of both the WDS-EPMA measurements and LA-ICP-MS measurements. The yellow letters indicate what WDS-EPMA measurements are taken in a particular shard. The red capital red letters and corresponding red circles indicate what LA-ICP-MS measurement is taken in a particular shard and the location of the laser spot.

SE map mount 1

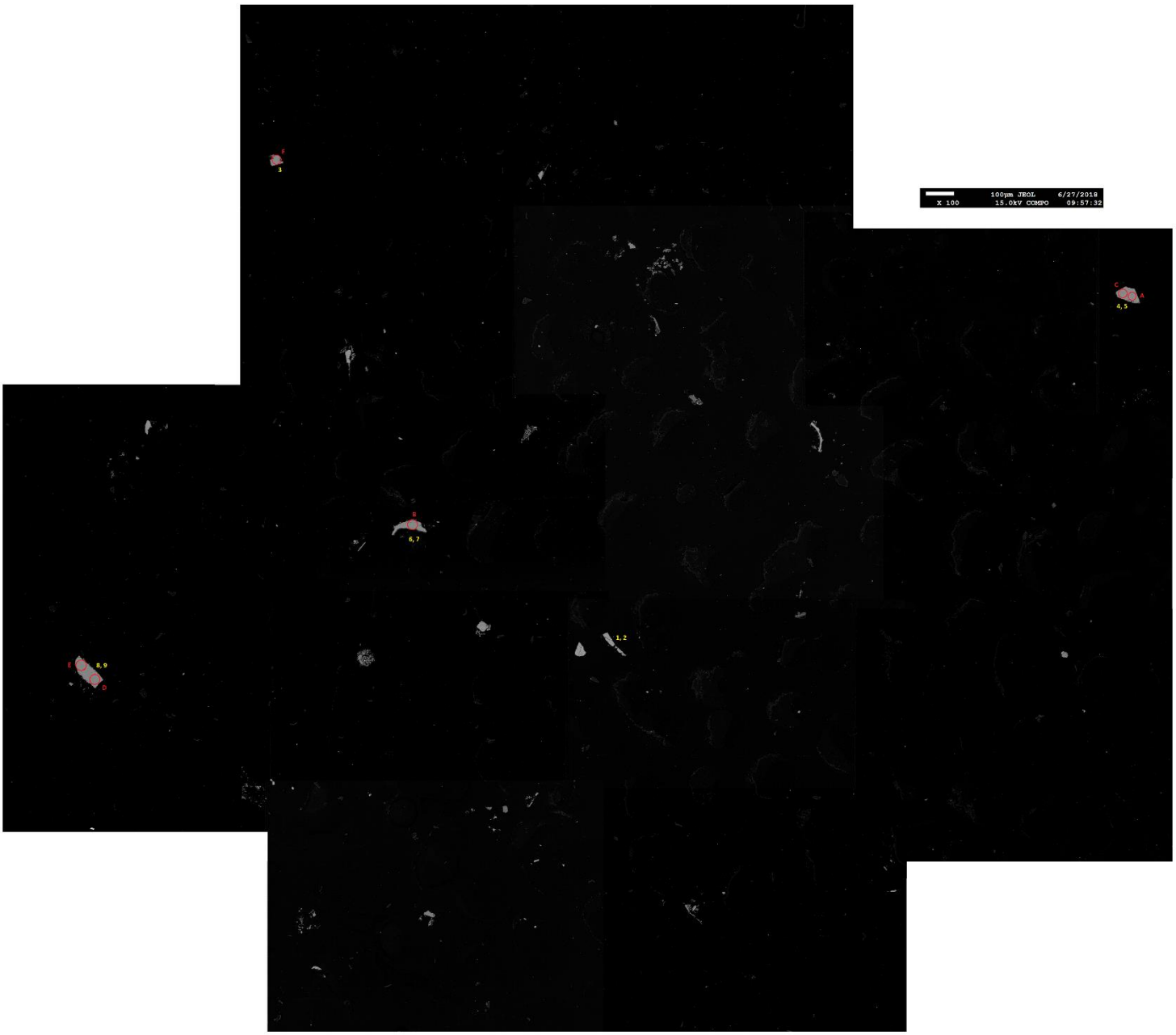

SE map mount 2

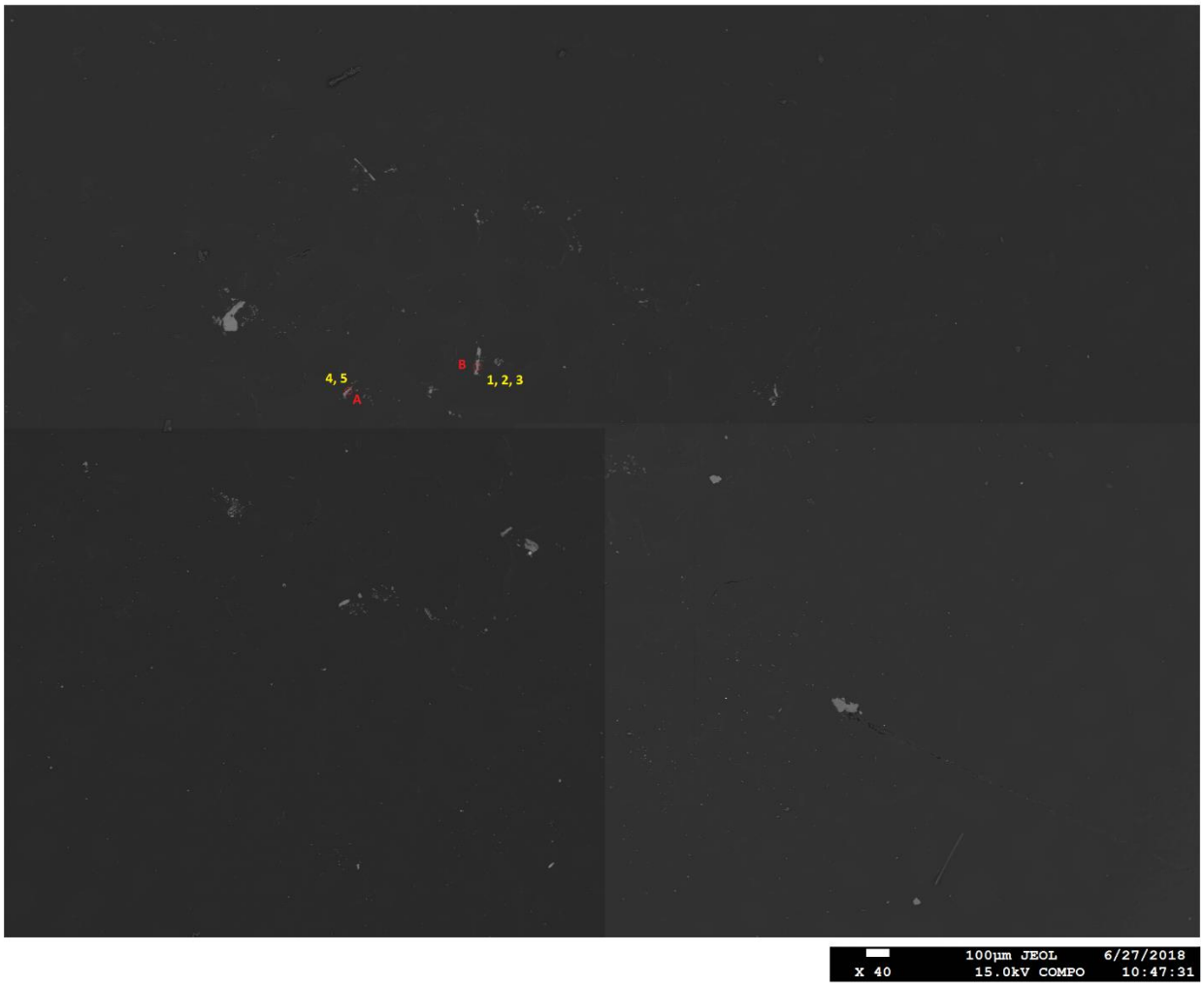

SE map mount 3

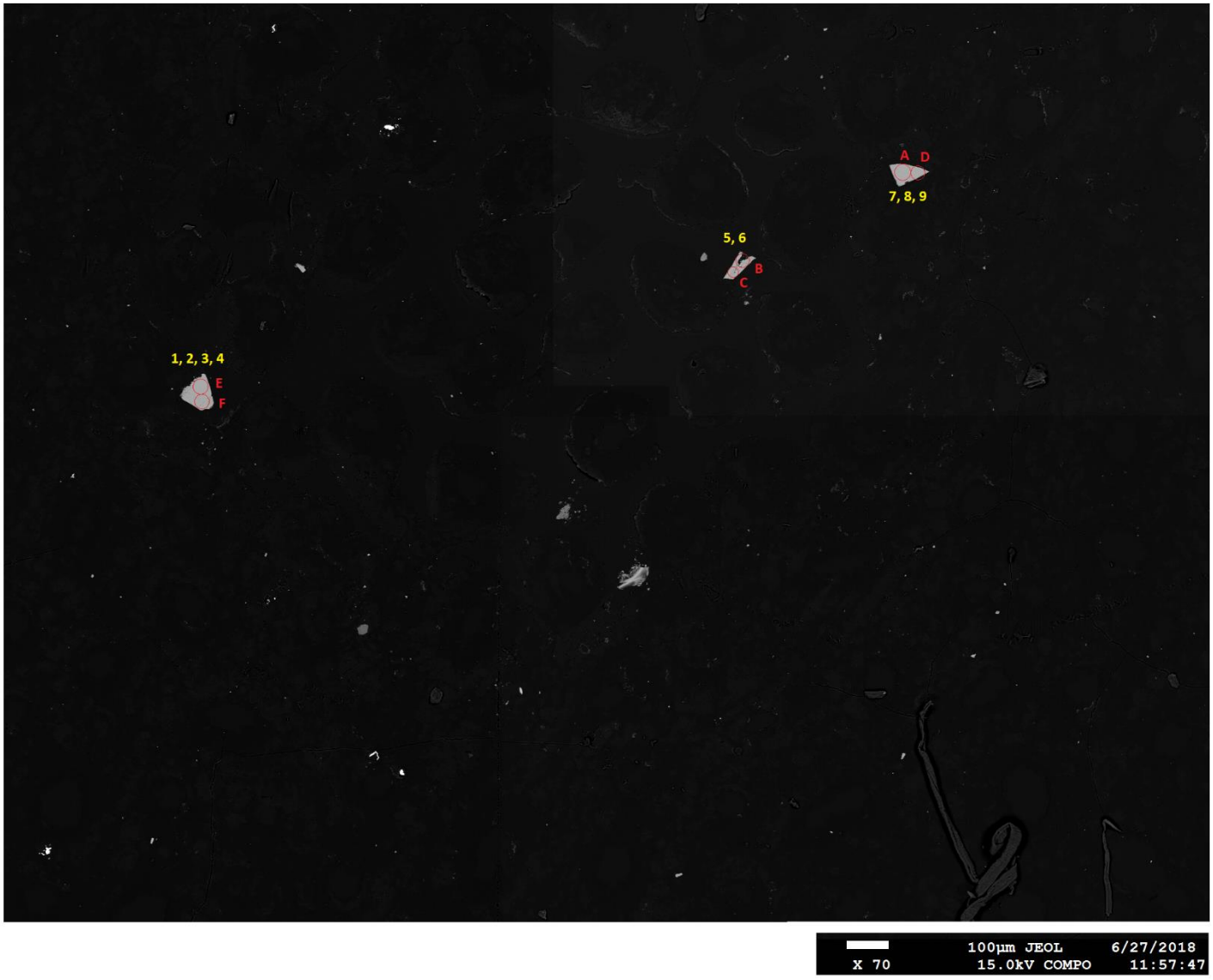

SE map mount 4

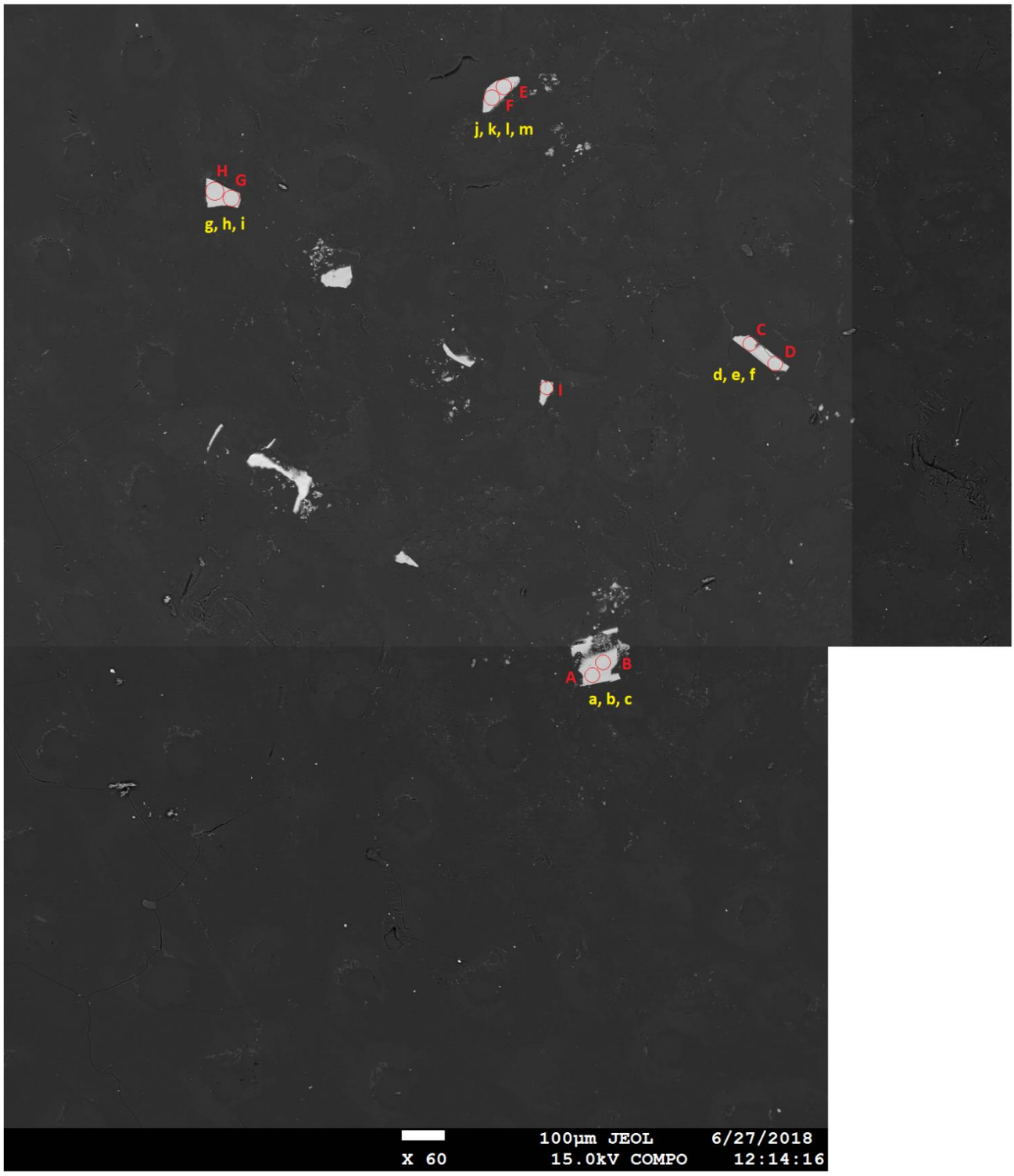

Appendix E

Additional information regarding LA-ICP-MS measurements. The first page includes the measurements of V and Cr (not shown in table 8) and their corresponding 1σ values, as measured by LA-ICP-MS and calculated by GLITTER. The second page shows a table of all 1σ values corresponding to the measurements of table 8.

	V	Cr
1a	<0.24	<0.82
1c	<0.57	<2.05
1b	<1.42	19.87
1d	<0.59	<2.12
1e	<0.56	3.39
1f	3.23	32.09
2a	<1.77	<6.44
2b	2.51	<5.80
3a	<0.60	<1.96
3d	<0.99	<3.78
3b	<2.54	45.19
3e	<0.42	<1.69
3f	<0.46	2.75
4a	<0.89	<3.56
4b	38.02	52.53
4c	<2.37	<9.11
4d	<1.66	<7.31
4e	<0.95	4.14
4f	<0.59	<2.60
4g	<0.50	<2.15
4h	2.4	5.66
4i	<0.63	4.59
rejected data		
1g	<12.03	97.12
1h	<10.85	<41.47
3c	11.12	<21.00

Table of trace element concentrations of V and Cr, as measured by LA-ICP-MS. Values including < sign indicate that the trace element concentrations were below the detection limit.

	V	Cr
1a	0.24	0.83
1c	0.41	1.46
1b	1.19	4.57
1d	0.39	1.4
1e	0.38	1.39
1f	2.53	9.25
2a	1.34	4.88
2b	0.88	3.05
3a	0.43	1.46
3d	0.7	2.91
3b	2.07	8.82
3e	0.36	1.45
3f	0.35	1.47
4a	0.73	2.87
4b	4.72	6.96
4c	1.17	4.52
4d	0.83	3.71
4e	0.73	3.26
4f	0.54	2.42
4g	0.37	1.59
4h	0.6	2.14
4i	0.46	1.97
rejected data		
1g	16.65	60.5
1h	12.07	49.84
3c	4.63	15.65

Table of 1σ values of V and Cr, as calculated by GLITTER.

Table of corresponding 1σ values of trace element concentrations in table 8.

	Rb	Sr	Y	Zr	Nb	Cs	Ba	La	Ce	Pr	Nd	Sm	Eu	Gd	Tb	Dy	Ho	Er	Tm	Yb	Lu	Hf	Ta	Pb	Th	U
1a	3.0	4.6	4.5	43.5	7.3	0.1	37.0	3.2	6.1	1.1	9.5	1.4	0.4	1.6	0.3	1.5	0.3	0.9	0.2	1.0	0.1	1.6	0.5	0.7	0.5	0.2
1c	3.5	4.8	4.5	46.5	8.4	0.1	45.5	3.8	6.2	1.2	9.5	1.6	0.5	2.0	0.3	1.7	0.5	1.0	0.2	1.0	0.1	2.1	0.7	1.1	0.6	0.2
1b	3.5	2.6	6.8	24.5	5.7	0.3	38.5	3.7	6.5	1.4	10.4	2.6	0.8	2.9	0.7	3.2	0.8	1.8	0.5	2.3	0.3	1.9	0.7	1.6	0.7	0.3
1d	3.3	5.0	5.3	55.4	9.1	0.1	40.7	3.6	6.6	1.3	11.2	1.6	0.4	1.7	0.4	1.8	0.4	1.0	0.3	1.0	0.2	1.9	0.6	0.9	0.5	0.2
1e	3.4	4.7	4.9	50.4	8.3	0.1	43.3	3.5	6.1	1.2	10.4	1.6	0.5	1.6	0.3	1.8	0.4	0.9	0.3	0.9	0.1	1.8	0.6	0.9	0.5	0.2
1f	5.5	7.1	6.2	58.4	10.2	0.4	57.6	5.0	7.7	1.9	13.0	4.7	1.2	5.1	0.9	3.8	1.3	2.0	1.1	2.9	0.3	2.9	1.2	2.6	1.1	0.5
2a	4.6	6.0	7.1	73.9	13.9	0.2	64.3	5.2	8.1	1.7	15.8	3.1	1.0	4.6	0.9	3.1	0.7	1.9	0.6	1.9	0.3	3.3	1.1	1.7	0.9	0.4
2b	4.5	6.3	7.4	73.4	12.0	0.2	53.1	4.5	7.7	1.7	16.2	2.0	0.5	2.0	0.4	2.9	0.7	1.4	0.4	1.3	0.2	2.4	0.7	1.5	0.7	0.3
3a	4.1	6.2	7.7	81.3	13.4	0.1	59.0	4.5	7.1	1.5	16.2	2.0	0.6	2.4	0.5	3.0	0.6	1.2	0.4	1.7	0.2	2.9	1.0	1.1	0.7	0.3
3d	4.9	6.9	7.3	81.5	12.9	0.2	63.6	4.8	7.7	1.9	16.3	3.0	0.8	2.8	0.7	3.4	0.9	1.8	0.5	1.7	0.3	3.6	1.0	1.4	0.8	0.3
3b	9.4	8.4	7.7	72.0	11.3	0.4	67.8	5.4	7.9	2.0	15.7	3.5	1.1	4.0	0.7	5.7	0.9	2.8	0.7	2.4	0.4	2.7	1.0	2.6	1.0	0.5
3e	4.2	6.9	8.7	89.5	14.3	0.2	64.0	4.8	7.5	1.8	18.0	2.0	0.7	3.0	0.5	2.6	0.8	1.4	0.4	1.8	0.2	2.9	0.9	1.2	0.7	0.3
3f	4.5	7.4	9.1	101.7	16.0	0.2	71.1	5.3	7.6	1.9	20.5	2.3	0.5	2.6	0.5	3.1	0.7	1.8	0.3	1.8	0.2	3.5	1.2	1.7	0.8	0.3
4a	5.1	7.3	8.7	87.7	14.0	0.2	69.2	5.5	8.4	2.2	19.7	2.8	0.7	3.0	0.7	2.4	0.7	1.9	0.5	2.3	0.2	3.1	0.9	1.8	0.8	0.4
4b	7.9	6.2	5.8	60.9	9.1	0.9	77.9	4.9	6.6	1.5	15.4	2.1	0.5	3.4	0.4	3.8	0.8	2.0	0.6	2.0	0.2	2.2	0.9	2.4	0.9	0.4
4c	5.2	6.3	7.3	80.3	13.8	0.2	73.1	5.2	7.7	1.7	18.0	2.1	0.6	3.4	0.7	4.3	0.9	1.8	0.6	1.8	0.2	3.2	1.0	1.7	0.7	0.3
4d	4.9	6.3	7.3	84.7	14.4	0.2	73.3	5.2	7.8	1.8	20.1	2.3	0.6	4.2	0.5	3.8	0.7	1.6	0.5	1.6	0.2	2.8	1.1	1.3	0.8	0.3
4e	5.3	8.9	12.7	146.5	22.8	0.2	97.0	6.7	10.0	2.8	28.6	3.5	1.0	4.1	0.8	5.1	1.4	2.4	0.5	3.0	0.3	3.8	1.4	2.9	0.9	0.4
4f	4.7	7.4	10.9	137.4	24.4	0.2	98.1	6.1	7.8	2.2	28.1	3.1	0.9	4.0	0.7	4.7	0.9	1.7	0.5	2.8	0.4	5.5	1.6	1.8	0.8	0.3
4g	5.1	6.3	7.9	95.4	17.4	0.2	103.2	6.4	7.6	1.8	19.0	2.6	0.8	3.7	0.7	4.9	0.9	1.8	0.3	1.6	0.3	4.7	1.6	2.2	0.9	0.3
4h	5.5	9.8	14.3	177.8	27.5	0.2	95.5	6.5	10.3	3.0	41.2	3.9	1.0	3.6	0.7	5.1	0.9	2.8	0.6	3.4	0.4	5.3	1.7	2.4	0.9	0.3
4i	5.8	8.2	9.7	99.8	13.4	0.2	86.3	6.7	9.2	2.4	24.3	2.6	0.6	3.2	0.6	5.6	1.1	1.9	0.4	1.8	0.2	2.6	0.9	1.7	0.8	0.3
rejected data																										
1g	18.4	11.6	8.2	36.1	8.2	2.0	64.3	6.4	9.0	2.9	15.4	1.5	5.3	9.8	0.6	14.1	0.5	0.8	0.8	10.2	1.6	0.7	2.9	7.4	2.2	3.1
1h	12.1	13.0	11.0	63.0	12.2	1.7	81.3	9.0	12.4	3.7	20.1	14.8	3.1	18.6	2.3	12.1	2.8	7.3	4.3	15.6	1.0	5.6	2.2	8.0	2.5	1.3
3c	7.1	9.2	9.1	98.5	18.2	0.6	70.2	5.8	10.5	2.5	26.0	5.5	1.4	4.6	1.2	6.5	1.7	4.8	1.6	4.3	0.5	3.9	1.4	4.3	1.3	0.7